ELSEVIER

International Journal of Mass Spectrometry 198 (2000) 137–163

International Journal of Mass Spectrometry

Review Article

Gas-phase enantioselectivity

A. Filippi[a], A. Giardini[b], S. Piccirillo[c], M. Speranza[a,*]

[a]*Dipartimento di Studi di Chimica e Tecnologia delle Sostanze Biologicamente Attive, Università di Roma "La Sapienza," 00185 Roma, Italy*

[b]*Dipartimento di Chimica, Università di Roma "La Sapienza," 00185 Roma, Italy*

[c]*Dipartimento di Scienze e Tecnologie Chimiche, Università di Roma "Tor Vergata," Roma, Italy*

Received 27 December 1999; accepted 31 January 2000

Abstract

Determination of the intrinsic noncovalent interactions governing chiral recognition in diastereomeric complexes constitutes the basis for understanding information transfer between molecules in living systems as well as in synthetic supramolecular structures. The most important experimental methodologies so far employed for this task are illustrated in the present review. Emphasis is put on the principles and the applications of techniques, such as radiolysis, Fourier transform ion cyclotron resonance (FTICR) and collision-induced dissociation (CID) mass spectrometry, and resonance-enhanced multiphoton ionization time-of-flight (REMPI-TOF) spectroscopy, that allow measurement of the relative stability of diastereomeric ion/molecule and molecule/molecule complexes and quantification of the short-range forces controlling their enantioselective evolution to products. (Int J Mass Spectrom 198 (2000) 137–163) © 2000 Elsevier Science B.V.

Keywords: Gas-phase enantioselectivity; Noncovalent interactions; Mass spectrometry; Radiolysis; Resonance-enhanced multiphoton ionization time-of-flight (REMPI-TOF) spectroscopy

1. Introduction

The capacity of a chiral molecular system (C) to specifically recognize the (*R*)-(R) and (*S*)-enantiomer (S) of an optically active compound is the basis of many important processes in chemistry (asymmetric synthesis, chiral chromatography, chiral NMR, etc.) and biology (enzymatic catalysis, etc.). The recognition mechanism involves the aggregation of the chiral selector C, either charged or neutral, and the enantiomeric pair R/S into two diastereomeric molecular complexes [CR] and [CS] held together by a different combination of noncovalent intermolecular interactions [1] and, therefore, endowed with different stability (thermodynamic enantioselectivity, K_R versus K_S) and reactivity (kinetic enantioselectivity, k_R versus k_S) [Eq. (1)]

* Corresponding author. E-mail: speranza@axrma.uniroma1.it

PII S1387-3806(00)00196-2

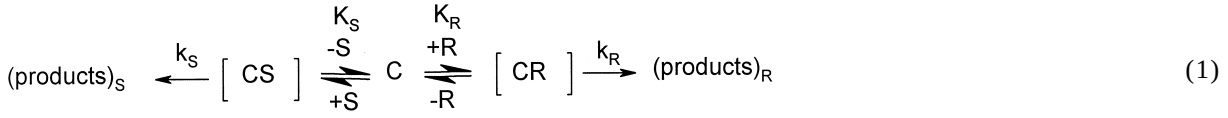

(1)

Quantification of noncovalent interactions in diastereomeric aggregates in the condensed phase represents a formidable task because of the transient character of the adducts and the unavoidable interference from the medium [1]. To overcome these difficulties, increasing attention is being paid to gas-phase techniques, chiefly mass spectrometry (MS). In fact, these techniques allow observation of long-lived diastereomeric aggregates and evaluation of their intrinsic interactions by eliminating the interfering effect of the solvent.

A crucial requisite for a correct application of MS to chiral discrimination is that the optically active moieties in the ionic aggregates $[CR]^+$ and $[CS]^+$ must retain their original configuration. As any other achiral physical probe, MS is inherently unable to ensure the fulfillment of this condition. Some insights may be obtained by the use of a complementary gas-phase kinetic methodology, i.e. the radiolytic technique, that allows generation of chiral ion/molecule complexes and structural analysis of their neutral products. The first part of this review will be devoted to this problem.

Most intensive MS studies on gas-phase chiral recognition have been carried out by using fast atom bombardment (FAB) or electrospray ionization (ESI) mass spectrometry, where the diastereomeric aggregates under investigation arise from desorption or vaporization of C and R/S dissolved in a liquid matrix. In general, either R or S is isotopically labeled so that the corresponding adducts $[CR]^+$ and $[CS]^+$ and their fragments can be mass discriminated. Despite the recognized versatility of FAB and ESI as fast analytical tools for monitoring enantiomeric excess, an ambiguity remains regarding the environment in which chiral recognition occurs, whether in the bulk of the matrix, in its selvedge vaporization region, or in the gas phase. Furthermore, neither technique ensures attainment of the equilibrium between $[CR]^+$ and $[CS]^+$ so that quantitative interpretation of their fragmentation patterns in terms of Eq. (1) is precluded. For these reasons, the description of the various FAB and ESI applications to chiral discrimination, whose continuous progress has been repeatedly outlined [2], is beyond the specific purposes of this review and will not be reported here.

The same restriction applies to the enantiodifferentiation observed in the chemical ionization (CI) mass spectrometry of chiral molecules. The majority of these studies concern the enantioselectivity of a chiral multifunctional molecule, such as dialkyl tartrate, when it selfassembles around a charged achiral core, e.g. a proton or an ammonium ion [3]. Other studies simply report the phenomenological differences in the CIMS ion patterns of chiral molecules, such as (+) and (−) isopinocampheol, when using a chiral CI reagent, such as (*R*)-(−)-2-amino-propan-1-ol [4]. Unlike FAB and ESI experiments, chiral recognition by CIMS *does* refer to the behavior of diastereomeric aggregates in the gas phase, but again it *does not* ensure attainment of the equilibrium between $[CR]^+$ and $[CS]^+$. This is demonstrated, for instance, by the net discrepancy between the $\Delta\Delta G = RT \ln(K_R/K_S) = 1.2$ KJ mol^{-1} ($[C]^+$ = protonated *L*-dialkyltartrate; S = *L*-dialkyltartrate; R = *D*-dialkyltartrate; k_R and $k_S = 0$; Eq. (1)), measured for the formation of the proton bound dimers $[CR]^+$ and $[CS]^+$ in CIMS experiments, and the corresponding value of 2.7 KJ mol^{-1}, obtained by Fourier transform ion cyclotron resonance (FTICR) mass spectrometry under equilibrium conditions [5].

For these reasons, the second part of this review is intended to focus exclusively on those MS procedures, such as FTICR or collision induced dissociation (CID) mass spectra, allowing unequivocal measurements of the kinetics or thermodynamics associated with the competing paths of Eq. (1).

The last part of the review will deal with the measurement of enantioselectivity in the formation of neutral diastereomeric aggregates [CR] and [CS] in

the isolated state. The method involves the use of laser-induced fluorescence (LIF) or resonance-enhanced multiphoton ionization (REMPI) processes coupled with MS detection.

2. Gas-phase rearrangements in chiral ion/molecule complexes by the radiolytic method

The growing impact of MS as an analytical tool for chiral recognition demands precise information on the stereochemistry of optically active ions in the gas phase and in particular, on their conceivable rearrangement in the collision complex with a neutral molecule. Until several years ago, this matter was virtually unexplored. The main reason is that the stereochemical study of a gas-phase ion/molecule reaction involving chiral reactants requires the combined application of specific kinetic approaches, e.g. the radiolytic technique [6], and advanced analytical tools, e.g. chiral chromatography, that allow isolation of the neutral products of the reaction and determination of their structure and configuration. The recent application of this integrated methodology led to the results outlined in this section. Their simple extension to processes occurring in the source of a mass spectrometer must be taken with a great deal of caution because of the largely different pressure regimes operating in radiolysis (10 Torr—several atmospheres) and in MS (<10 Torr). The high-pressure regime typical of radiolytic experiments allows efficient collisional thermalization of the ion/molecule adducts prior to their conversion to products. The same conditions can hardly be attained at the low pressures of MS experiments and, therefore, the probability of extensive intracomplex rearrangements, including racemization of the chiral moieties, may substantially increase.

2.1. Acid-induced racemization and isomerization of chiral allylic alcohols

Bimolecular nucleophilic displacements in allylic compounds are known to proceed via the four possible pathways shown in Scheme 1.

The existence itself of the S_N2' mechanism, the question of its concertedness, and the origin of its stereochemistry, have been a matter of lively debate for the last half century [7]. The controversy was continuously sustained by the paucity of firm proofs of the S_N2' mechanism in solution and by the coincidence of the S_N2' products with those arising from alternative competing mechanisms, i.e. S_N1, unimolecular rearrangement of the starting alcohol before substitution, and of its derivatives after S_N2 substitution, etc.

This ambiguity was recently removed by the results of a comprehensive investigation of the gas-phase acid-induced nucleophilic substitution on several allylic alcohols showing that the concerted S_N2' reaction competes with the classical S_N2 pathway in the absence of solvation and ion-pairing factors [8]. Assessment of the stereochemistry of the gas-phase S_N2' reactions in these systems requires a detailed knowledge of the extent of conceivable rearrangements in the starting intermediates **1** prior to nucleophilic attack (Scheme 2).

To this purpose, the oxonium ion **1** (A = H; Alk = ethyl; Alk′ = methyl) has been generated in the gas phase (720 Torr) by protonating the corresponding allylic alcohol with $C_nH_5^+$ (n = 1, 2) and s-$C_3H_7^+$ obtained, respectively, by γ radiolysis of CH_4 and C_3H_8. Ion **1** was found to undergo appreciable inversion to **2** (A = H; Alk = ethyl; Alk′ = methyl) and isomerization to racemic **3** (A = H; Alk = ethyl; Alk′ = methyl) in yields (Y_{racem} and Y_{isom}, respectively) that depend on the temperature of the gaseous mixture (40–120 °C) and on the reaction time t. This is defined by the concentration of the powerful $(CH_3)_3PO_4$ base [proton affinity (PA) = 212 kcal mol^{-1}] [9] deliberately added to the system. The experimental results, combined with ab initio calculations on the model [$C_3H_5^+/H_2O$] system, point to the rearrangement of **1** proceeding through structurally distinct intermediates **I** and **II** characterized by site-specific hydrogen bonding (Scheme 2). If the probabilities of conversion of complex **I** to the **1**/**2** enantiomeric pair and to isomer **3** are equal, the rate constant for the formation of **I** from **1** can be expressed by $k_{(I)} = t^{-1} \ln(1 - 2Y_{isom})^{-1}$ and that for

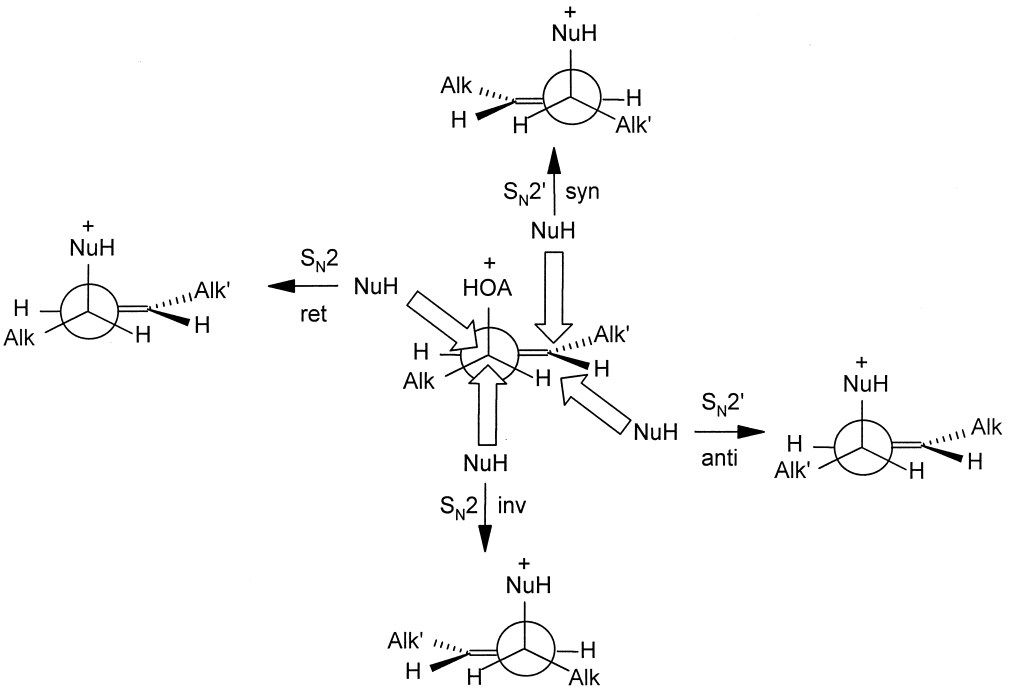

Scheme 1.

the formation of **II** by $k_{(\mathbf{II})} = t^{-1} \ln[1 - 2(Y_{\text{racem}} - 0.5Y_{\text{isom}})]^{-1}$. The relevant values are plotted, respectively, in Figs. 1 and 2 as a function of the reaction temperature.

The observation that essentially the same rate constants are measured in methane and propane at 40 and 100 °C demonstrates that the starting oxonium ion **1** is in thermal equilibrium with the bulk gas and that its unimolecular rearrangement depends exclusively on the reaction temperature.

Similar plots have been obtained for the gas-phase rearrangement of **1** (A = CH_3; Alk = ethyl; Alk′ = methyl; Scheme 2) and **2** (A = CH_3; Alk = methyl; Alk′ = ethyl; Scheme 2) in 720 Torr methyl chloride in the temperature range 40–120 °C [10]. Regression analysis of the relevant Arrhenius curves leads to the activation parameters listed in Table 1.

The activation parameters of Table 1 suggest that the energy, the charge distribution, and the location of the relevant transition structures (TS) along the reaction coordinate depend significantly on the nature of the moving AOH moiety. When A = H, the racemization and isomerization TS are located early on the reaction coordinate, whereas they are late with A = CH_3 and are characterized by comparatively stronger H-bond interactions.

The limited extent of intramolecular rearrangements undergone by the chiral oxonium ions **1** and **2** at 720 Torr and at 40 °C (Table 1) allows for their use in probing the regio- and stereochemistry of the displacement reactions of Scheme 1. In this case, the allylic alcohol (precursor of the chiral oxonium ions **1** and **2**) acts as the nucleophile NuH [11]. The relevant results are condensed in Chart 1. They are fully consistent with modern concepts [7(c)–8] pointing to concerted acid-catalyzed S_N2' reactions that are feasible in the gas phase and that efficiently compete with the classical S_N2 processes. According to these concepts, a preferred *anti*-relationship between the NuH and the leaving group is observed in gas-phase S_N2'. The relevant TS is only marginally influenced by stereoelectronic factors, whereas it is strongly favored by the lack of the nonbonding and repulsive Coulombic interactions between NuH and the leaving

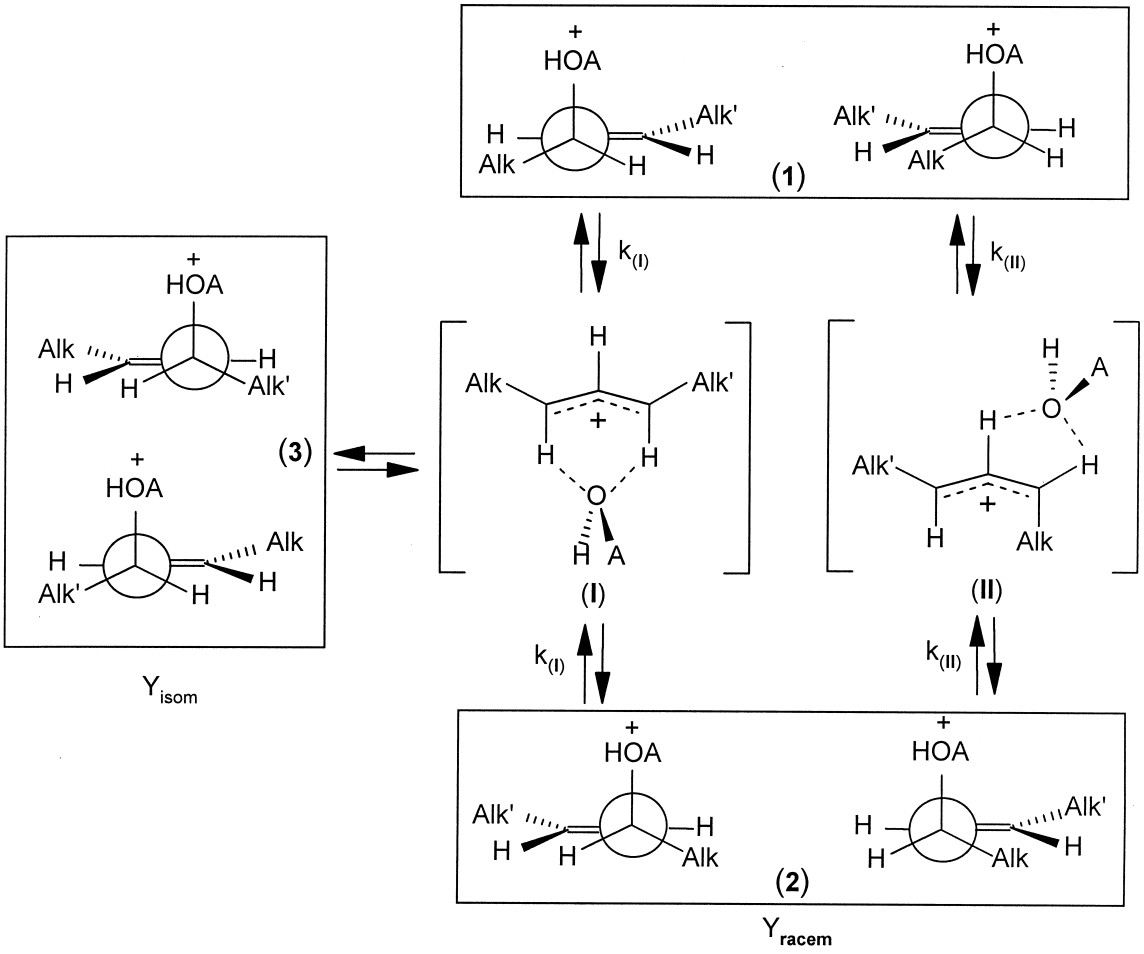

Scheme 2.

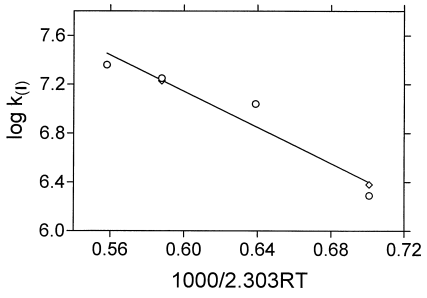

Fig. 1. Arrhenius plots for the formation of intermediate **I** in 720 Torr of methane (circles) and propane (diamonds).

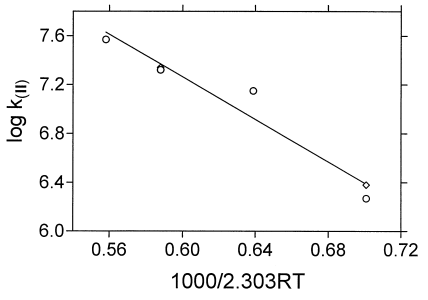

Fig. 2. Arrhenius plots for the formation of intermediate **II** in 720 Torr of methane (circles) and propane (diamonds).

Table 1
Arrhenius parameters for the gas-phase racemization and isomerization of chiral ions **1** and **2**

Reaction	Arrhenius equation[a]	Correlation coefficient (r)	ΔH* (kcal mol^{-1})	ΔS* (cal mol^{-1} K^{-1})
1(A = H; alk = C_2H_5; alk′ = CH_3) → **I**	log $k_{(I)}$ = (11.6 ± 0.4) − (7.4 ± 0.5)x	0.960	6.7 ± 0.5	−7.9 ± 2.4
1(A = H; alk = C_2H_5; alk′ = CH_3) → **II**	log$k_{(II)}$ = (12.5 ± 0.4) − (8.7 ± 0.6)x	0.963	8.0 ± 0.6	−3.7 ± 2.8
1(A = CH_3; alk = C_2H_5; alk′ = CH_3) → **I**	log $k_{(I)}$ = (10.6 ± 0.4) − (5.4 ± 0.5)x	0.978	4.7 ± 0.5	−12.4 ± 2.1
1(A = CH_3; alk = C_2H_5; alk′ = CH_3) → **II**	log$k_{(II)}$ = (10.1 ± 0.4) − (6.3 ± 0.5)x	0.960	5.6 ± 0.5	−14.6 ± 2.1
2(A = CH_3; alk = CH_3; alk′ = C_2H_5) → **I**	log $k_{(I)}$ = (10.9 ± 0.4) − (5.8 ± 0.5)x	0.987	5.1 ± 0.5	−11.2 ± 1.9
2(A = CH_3; alk = CH_3; alk′ = C_2H_5) → **II**	log$k_{(II)}$ = (10.3 ± 0.4) − (6.5 ± 0.6)x	0.988	5.8 ± 0.6	−13.6 ± 2.1

[a] x = 1000/2.303 RT.

group, which usually play a critical role in the gas phase [7(c)–(e)].

2.2. Acid-induced ring opening of chiral alkene oxides

The detailed knowledge of ring opening in 1,2-epoxides represents the basis for understanding the mutagenic and carcinogenic activity of aromatic hydrocarbons and their metabolites in biological tissues. The mechanism and the stereochemistry of this class of reactions are heavily affected in solution by environmental factors. For instance, depending upon the pH of the reaction medium, alcoholysis of epoxides may follow either a unimolecular or a bimolecular pathway with a stereochemistry ranging from complete retention to complete inversion of configuration. Discrimination between intrinsic structural and environmental factors on the ring opening of epoxides arises from a detailed investigation of the reaction in the gas phase, where the nature of the active intermediates is well defined and their evolution to products is unaffected by solvation and ion-pairing phenomena [12].

Gas-phase acid-induced ring opening of enantiomerically pure 1,2-propene (**4** and **5**) and styrene oxides (**6** and **7**) has been investigated at room temperature using $CH_3{}^{18}OH$, CD_3OH, and $H_2{}^{18}O$ as nucleophiles, and $C_nH_5^+$ (n = 1, 2) and $(CH_3)_2F^+$ as gaseous acids generated by γ radiolysis of CH_4 and CH_3F (720 Torr), respectively [13,14]. No racemization of the starting chiral epoxide is observed under all experimental conditions. Therefore, the ring opening takes place on the O-protonated (or O-methylated) **4**–**7** retaining the original configuration of their precursors. Ring opening proceeds via two different reaction pathways. In the $CH_3F/H_2{}^{18}O$ systems, the reaction follows the intracomplex mechanism depicted in Scheme 3. It involves protonation of the oxygen of the epoxide by the $CH_3{}^{18}OH_2^+$ ion, generated in the gaseous mixture by $(CH_3)_2F^+$ methylation of $H_2{}^{18}O$. The neutral $CH_3{}^{18}OH$ molecule, arising

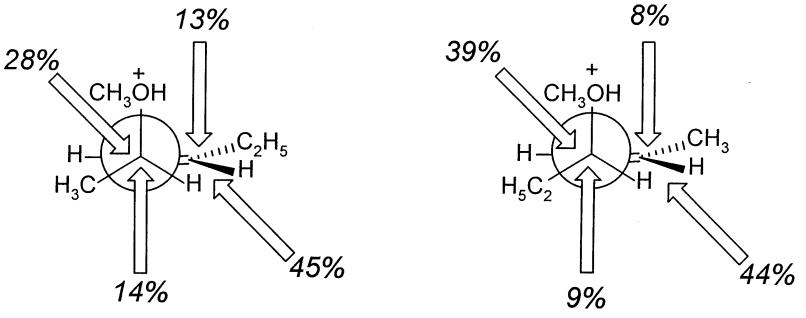

Chart 1.

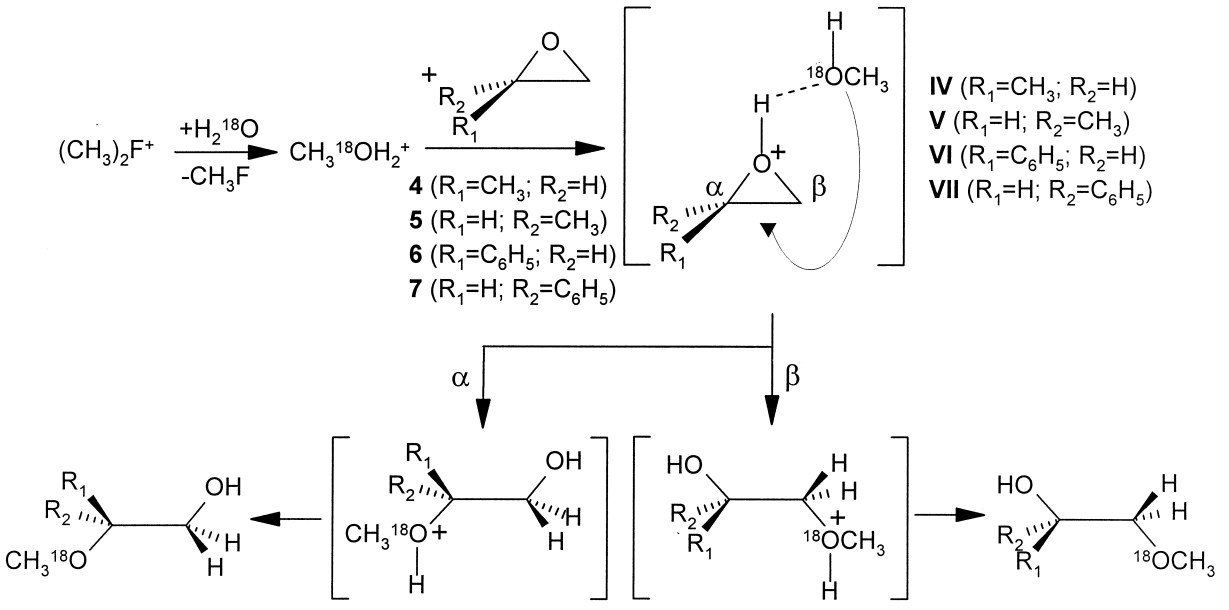

Scheme 3.

from the proton transfer, moves around the oxonium ions ($k < 10^8$ s^{-1}) before attacking their ring carbons. The attack exclusively occurs at the α carbon of **VI** and **VII** with slightly predominant inversion of the configuration (55–67%). However, with **IV** and **V**, the attack takes place at both ring carbons ($\alpha/\beta = 0.72 \pm 0.05$) with exclusive inversion of their configuration.

In the $CH_4/CH_3{}^{18}OH$ systems, the intracomplex pathway is preceded by the extracomplex attack of an external $CH_3{}^{18}OH$ molecule. Both the intracomplex and the extracomplex pathways display the same regio- and stereoselectivity. The different regio- and stereoselectivity observed for **IV/V** and **VI/VII** is explained in terms of a different extent of C_α–O bond rupture in the relevant TS. Ring-opening of **VI/VII** involves a loose TS characterized by extensive C_α–O bond cleavage promoted by conjugative delocalization of the C_α positive charge over the phenyl ring. The same stabilization mechanism is not operative in the ring opening of **IV/V** whose TS is therefore characterized by a much less advanced C_α–O cleavage.

2.3. Intracomplex arenium ion-chiral molecule reactions

Knowledge of the configuration and the relative spatial arrangement of the reactants confined in an ion/molecule complex is of crucial importance for assessing the kinetics and the mechanism of its evolution to products. Direct experimental information on these points is very scarce, but some insights are available with regard to gas-phase electrophilic aromatic substitutions

$$C_6H_7^+ + C_4H_9Cl \rightarrow [C_6H_7^+ \cdot C_4H_9Cl] \rightarrow [C_6H_6 \cdot C_4H_9ClH^+] \rightarrow C_{10}H_{15}^+ + HCl \quad (2a)$$

$$C_6H_7^+ + C_4H_9Cl \rightarrow [C_6H_7^+ \cdot C_4H_9Cl] \rightarrow [C_6H_6 \cdot C_4H_9^+ \cdot HCl] \rightarrow C_{10}H_{15}^+ + HCl \quad (2b)$$

At 300 K and under FTICR conditions, the benzenium ion $C_6H_7^+$ reacts with 2-chlorobutane C_4H_9Cl to give the $C_{10}H_{15}^+$ ion with a rate constant of 5×10^{-11} cm^3 $molecule^{-1}$ s^{-1}, corresponding to a collision efficiency of 2.5% [Eqs. (2)] [15]. No information is

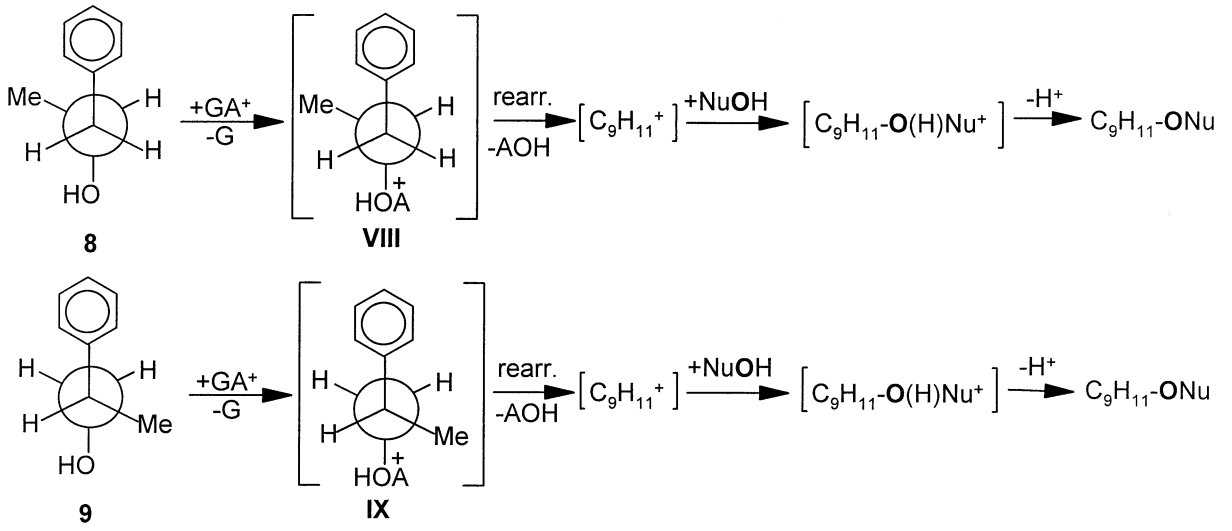

Scheme 4.

available from this experiment regarding the detailed path of formation of $C_{10}H_{15}^+$, whether via Eq. (2a) or (2b). Besides, no information is available regarding the spatial relationship of the species present in the second complex of Eqs. (2). These are mechanistically relevant questions concerning the nature ("loose" versus "structured") of gaseous ion/molecule complexes that are structurally analogous to those involved in the classical Friedel–Crafts arene alkylation by alkyl halides. To answer these questions, the $^{12}C_6H_6D^+$ ion, obtained from $^{12}C_6H_6$ by deuteronation with radiolytic $C_nD_5^+$ ($n = 1, 2$), was allowed to react at 700 Torr with (*R*)-(−)-2-chlorobutane [16]. The 2-phenylbutane recovered among the radiolytic products was found to contain ∼10% deuterium. Its formation must necessarily proceed through Eqs. (2) because the alternative route involving deuteronation of (*R*)-(−)-2-chlorobutane and subsequent DCl displacement by $^{12}C_6H_6$ leads only to unlabeled 2-phenylbutane. The observation that complete racemization accompanies formation of deuterated 2-phenylbutane points to its formation as proceeding exclusively via Eq. (2b). Another relevant point concerns the spatial correlation of the reactants in the three-body adduct $[C_6H_5D \cdot C_4H_9^+ \cdot ClH]$ of Eq. (2b). If the electrophile $C_4H_9^+$ moiety maintains, in the complex, a fixed juxtaposition relative to the arene (a "structured" complex) until substitution takes place, a marked stereoselectivity would be observed in contrast to the experimental evidence. This is instead consistent with a complex where the moieties are not constrained in a fixed geometry (a "loose" complex).

2.4. Wagner–Meerwein rearrangements in chiral ions

In view of the considerable interest in ion/molecule complexes involved in gas-phase analogs of solvolytic reactions [17], a sustained research effort has been recently directed to the study of Wagner–Meerwein rearrangements in cationized β-arylalkyl systems, under conditions excluding nucleophilic assistance by the solvent (which in these systems normally interferes with anchimeric assistance of groups adjacent to the reaction center). In particular, a great deal of effort has been directed to the assessment of the kinetics and the stereochemistry of the unimolecular H_2O loss from the chiral oxonium ions **VIII** and **IX** (A = H or CH_3; Scheme 4) [18].

Ions **VIII** and **IX** arise from the corresponding chiral alcohols **8** and **9** by reaction with gaseous acids (GA^+), either $C_nH_5^+$ ($n = 1, 2$) (A = H) or $(CH_3)_2F^+$ (A = CH_3), formed respectively by γ ra-

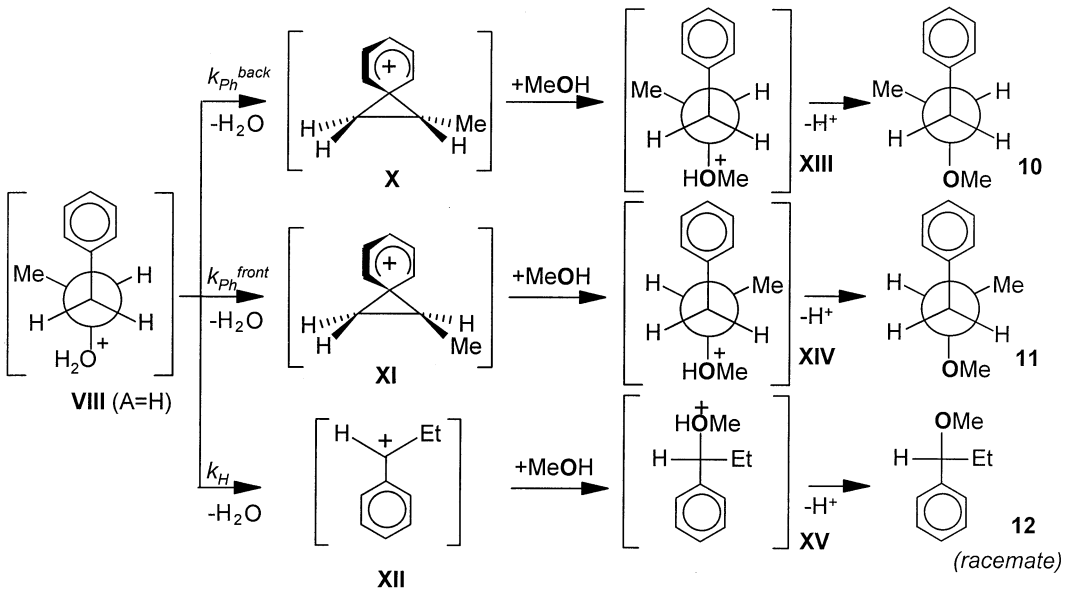

Scheme 5.

diolysis of CH_4 and CH_3F (750 Torr). The reaction sequences of Scheme 4 have been investigated in the temperature range 25–140 °C, in the presence of $CH_3{}^{18}OH$ or $H_2{}^{18}O$, as nucleophiles (Nu**O**H). The experimental results conform to the unimolecular loss of H_2O from **VIII** and **IX** (A = H), anchimerically assisted by all the groups adjacent to the leaving moiety (Schemes 5 and 6). Anchimeric assistance to the CH_3OH loss from **VIII** and **IX** (A = CH_3) appears much less effective.

The linear Arrhenius plots of the $k_{Ph}^{back}/k_{Ph}^{front}$, k_{Ph}^{back}/k_H, and k_{Ph}^{front}/k_H ratios (Scheme 5) and of the k_{Ph}/k_{Me}, k_{Ph}/k_H, and k_{Me}/k_H ratios (Scheme 6), taken in the 25–140 °C interval, adhere to the differential activation parameters listed in Table 2.

From the reported values, the absolute activation energy for the backside phenyl, frontside phenyl, methyl, and hydrogen participation to the H_2O loss in **VIII** and **IX** (A = H) can be estimated as ranging around 9, 8, 4, and 2 kcal mol^{-1}, respectively.

Analysis of Table 2 indicates that in **VIII** and **IX** (A = H), the neighboring-group assistance is mainly controlled by entropic, rather than enthalpic factors. Furthermore, the counterintuitive observation that the frontside phenyl-group participation involves an activation barrier lower than that of the competing backside participation finds a rationale in the *gauche-anti* conformation of the oxonium ion **VIII** (A = H), most favored in the gas phase, and on the stabilizing electrostatic interactions between the leaving H_2O moiety and the ring of the phenonium ion in the transition structure **XVIII** (Chart 2).

Unequivocal characterization of the transition structures involved in the anchimeric assistance to H_2O loss from **VIII** and **IX** (A = H) is obtained by analysis of the relevant deuterium primary (PKIE) and secondary kinetic effects (SKIE). The pertinent data are reported in Tables 3 and 4.

Whereas the gas-phase β-D_1-PKIE, α-D_1-SKIE, and β'-D_3-SKIE values fall in the classical range of deuterium effects for analogous solvolytic processes, the relatively large values of $(\beta\text{-}D_1\text{-SKIE})_{Ph}$ reflect a convolution of the isotope effects for the competing backside[$(\beta\text{-}D_1\text{-SKIE})_{Ph}^{back} \leq 1$] and frontside phenyl-group participation [$(\beta\text{-}D_1\text{-SKIE})_{Ph}^{front} \approx 1.4$]. The deuterium PKIE and SKIE in Tables 3 and 4 are consistent with the corresponding activation parameters in Table 2 by indicating that the transition structures involved in the phenyl-group participation of Schemes 5 and 6 are characterized by partial

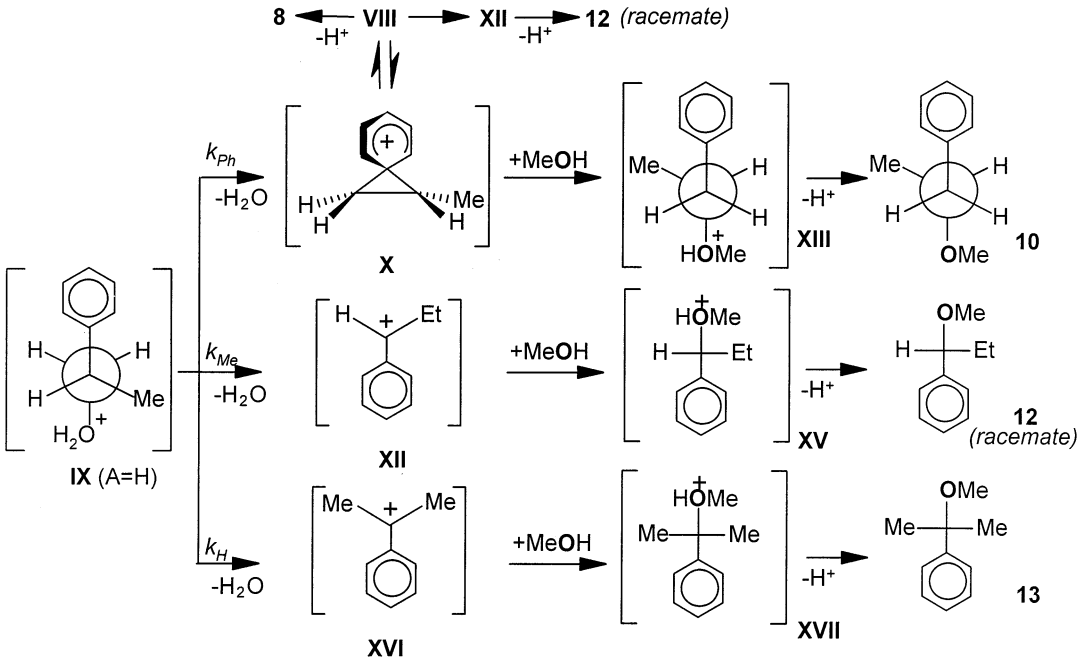

Scheme 6.

C_α–OH_2^+ bond cleavage coupled with weak Ph–C_α interaction. In contrast, β-hydrogen participation involves much tighter transition structures, characterized by significant H–C_α bonding and limited C_α–OH_2^+ bond cleavage. Finally, β-methyl group participation in **IX** involves borderline transition structures, in which intense Me–C_α bonding is coupled with a pronounced C_α–OH_2^+ bond elongation.

3. Gas-phase enantioselectivity by the mass spectrometric methods

As pointed out in the Introduction, this section is intended to focus exclusively on those mass spectrometric methodologies, i.e. FTICR and CID, that allow determination of the thermodynamic and kinetic parameters of Eq. (1).

Table 2
Differential Arrhenius parameters for the competing neighboring-group participation to the unimolecular H_2O loss in the chiral oxonium ions **VIII** and **IX**

Reaction	Arrhenius equation[a]	Correlation coefficient (r)
X ← VIII → XII	$\log (k_{Ph}^{back}/k_H) = (5.0 \pm 0.3) - (7.0 \pm 0.3)x$	0.960
XI ← VIII → XII	$\log (k_{Ph}^{front}/k_H) = (3.2 \pm 0.3) - (5.6 \pm 0.3)x$	0.964
X ← VIII → XI	$\log (k_{Ph}^{back}/k_{Ph}^{front}) = (1.7 \pm 0.5) - (1.3 \pm 0.5)x$	0.927
X ← IX → XII	$\log (k_{Ph}/k_{Me}) = (4.7 \pm 0.2) - (5.7 \pm 0.2)x$	0.997
X ← IX → XVI	$\log (k_{Ph}/k_H) = (6.0 \pm 0.2) - (7.1 \pm 0.2)x$	0.997
XII ← IX → XVI	$\log (k_{Me}/k_H) = (1.3 \pm 0.5) - (1.4 \pm 0.5)x$	0.906

[a] $x = 1000/2.303$ RT.

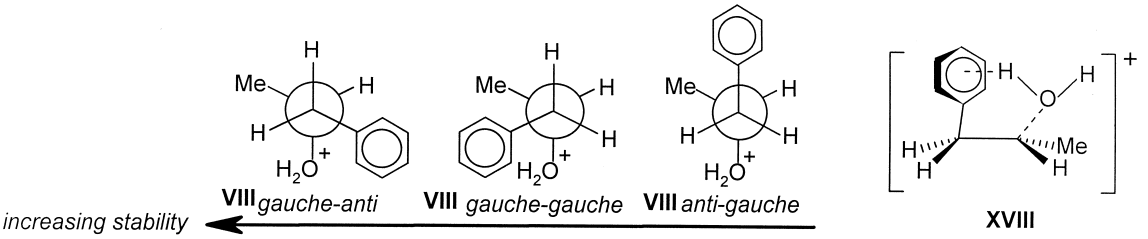

Chart 2.

3.1. Chiral ion/molecule association

The first quantitative FTICR study on asymmetric ion/molecule association involving chiral species was carried out by Nikolaev and co-workers [5], who determined the relative stability of the homochiral and the heterochiral dimers arising from self-CI of a 1:1 mixture of the *L* and the *D* enantiomers of dimethyl- (**14**) and diisopropyl-tartrate (**15**). The dimer chirality effect, expressed by the $Y = 2([\mathbf{14}\cdot\mathbf{14}\cdot H^+][\mathbf{15}\cdot\mathbf{15}\cdot H^+])^{1/2}/[\mathbf{14}\cdot\mathbf{15}\cdot H^+]$ ratio, was quantitatively evaluated at 20 °C and at different delay times (from 0.5 to 5 s) from the peak intensities of homogeneous and heterogeneous dimers. Although the corresponding peak intensities change appreciably with time, the *Y* ratio remains essentially constant at the values reported in Table 5. In the absence of chirality effects, the *Y* term must be the same for all four reactions of Table 5.

Under such conditions, the ratio of the *Y* terms of the *LL* and the *LD* systems is equal to the equilibrium constant *K* for the ligand exchange reaction: $L_{\mathbf{14}}L_{\mathbf{15}}H^+ + D_{\mathbf{15}} \Leftrightarrow L_{\mathbf{14}}D_{\mathbf{15}}H^+ + L_{\mathbf{15}}$. From the values in Table 5, $K = 0.33$ and the $\Delta G^0_{298} = -RT \ln K = 2.7$ KJ mol^{-1}. The lack of chirality effects observed when tartrates **14** and **15** are replaced by the *L* and the *D* enantiomers of methyl lactate, alanin-amide, and N-acetyl-α-methyl-benzylamine is attributed to their extensive racemization after protonation.

Table 3
Deuterium isotope effects involved in the competing neighboring group participations to H_2O loss from **VIII** (A = H) (Scheme 5)

Participating group	Kinetic isotope effect
Ph	$(\alpha\text{-}D_1\text{-SKIE})_{Ph} = 1.11 \pm 0.03$
Ph	$(\beta\text{-}D_1\text{-SKIE})_{Ph} = 1.23 \pm 0.03$
Ph	$(\beta'\text{-}D_3\text{-SKIE})_{Ph} = 1.06 \pm 0.04$
β-D	$(\beta\text{-}D_1\text{-PKIE})_{D} = 1.22 \pm 0.04$[a]
β-H	$(\alpha\text{-}D_1\text{-SKIE})_{H} = 1.09 \pm 0.03$
β-H	$(\beta\text{-}D_1\text{-SKIE})_{H} = 1.04 \pm 0.04$[a]
β-H	$(\beta'\text{-}D_3\text{-PKIE})_{H} = 1.08 \pm 0.04$
β-D	$(\beta\text{-}D_2\text{-PKIE})_{D} = 1.19 \pm 0.06$[b]
β-H	$(\beta\text{-}D_2\text{-SKIE})_{H} = 1.01 \pm 0.06$[b]

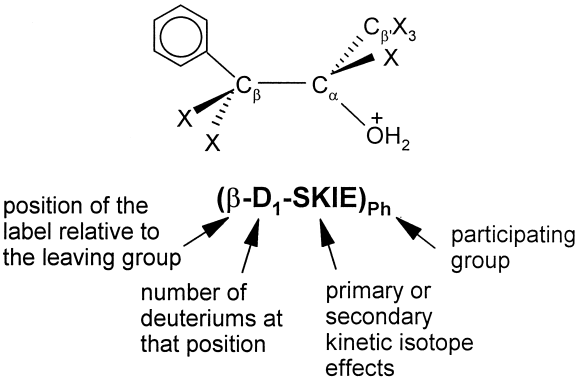

[a] β-H, spectator atom.
[b] β-D, spectator atom.

Table 4
Deuterium isotope effects involved in the competing neighboring group participations to H_2O loss from **IX** (A = H) (Scheme 6)

Participating group	Kinetic isotope effect
Ph	$(\alpha\text{-}D_1\text{-SKIE})_{Ph} = 1.12 \pm 0.02$
Ph	$(\beta\text{-}D_1\text{-SKIE})_{Ph} = 1.17 \pm 0.02$
Me	$(\alpha\text{-}D_1\text{-PKIE})_{Me} = 1.33 \pm 0.08$
Me	$(\beta\text{-}D_1\text{-SKIE})_{Me} = 1.05 \pm 0.03$
β-H	$(\beta\text{-}D_1\text{-PKIE})_{D} = 1.94 \pm 0.05$
β-H	$(\alpha\text{-}D_1\text{-PKIE})_{H} = 1.09 \pm 0.03$

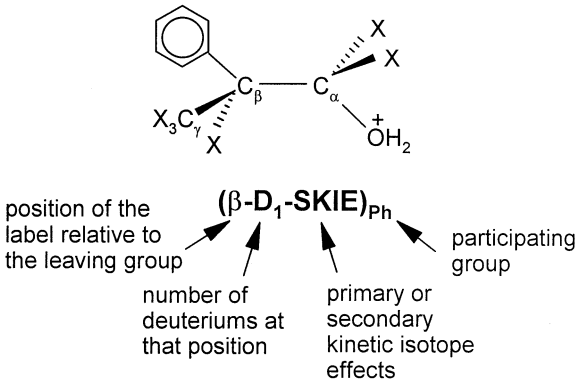

3.2. Chiral ligand exchange of proton-bound complexes

The FTICR technique has been employed to measure the gas-phase exchange equilibria of the (*R*)-($R_{\mathbf{XIX}}$) and (*S*)-1-naphthyl-ethylammonium cation **XIX** ($S_{\mathbf{XIX}}$) ligands between chiral (*S*,*S*)-dimethyldiketopyridino-18-crown-6 **16** and achiral 18-crown-6 **17** (Chart 3) [19].

The achiral crown ether **17** displays an affinity for $R_{\mathbf{XIX}}$ and $S_{\mathbf{XIX}}$ that is higher than that of the chiral crown ether **16**. The equilibrium constants for reactions (3) and (4) amount to 130 ± 15 and 567 ± 68, respectively, which correspond to a difference of 4.2 ± 0.4 KJ mol^{-1} between the stability of the hetero- $[\mathbf{16}\cdot R_{\mathbf{XIX}}]^+$ and the homochiral complex $[\mathbf{16}\cdot S_{\mathbf{XIX}}]^+$

$$[\mathbf{16}\cdot R_{\mathbf{XIX}}]^+ + \mathbf{17} \Leftrightarrow \mathbf{16} + [\mathbf{17}\cdot R_{\mathbf{XIX}}]^+ \quad (3)$$

Table 5
Average values of $Y = 2([\mathbf{14}\cdot\mathbf{14}\cdot H^+]x[\mathbf{15}\cdot\mathbf{15}\cdot H^+])^{1/2}/[\mathbf{14}\cdot\mathbf{15}\cdot H^+]$

Mixture	*Y*
$L_{\mathbf{14}} + L_{\mathbf{15}}$	2.8
$D_{\mathbf{14}} + L_{\mathbf{15}}$	8.4
$L_{\mathbf{14}} + D_{\mathbf{15}}$	8.3
$D_{\mathbf{14}} + D_{\mathbf{15}}$	2.7

$$[\mathbf{16}\cdot S_{\mathbf{XIX}}]^+ + \mathbf{17} \Leftrightarrow \mathbf{16} + [\mathbf{17}\cdot S_{\mathbf{XIX}}]^+ \quad (4)$$

This stability difference is greater than that measured in methanol solution (2.3 KJ mol^{-1}), but similar to that seen in CD_2Cl_2 (4.6 KJ mol^{-1}) [20]. This provides experimental support for the concept that solvation moderates those short-range intracomplex forces that play a major role in chiral discrimination, such as the π–π stacking interactions between the guest **XIX** and the host **16**.

With the same methodology, it was possible to quantify the gas-phase exchange equilibria of the (*R*)-enantiomer of the chiral amines **18–21** with protonated (*S*,*S*)- and (*R*,*R*)-dimethyldiketopyridino-18-crown-6 ethers (**XX**), generated by the ESI technique (Chart 4) [21].

One among **18–21** was introduced together with a reference achiral amine, i.e. isopropylamine or cyclohexylamine, into the FTICR cell, where they react with either $SS_{\mathbf{XX}}$ or $RR_{\mathbf{XX}}$ to form the corresponding adducts. The equilibrium constant for the exchange of the chiral and the achiral amine guests was determined and the enantioselectivity of the process was inferred from the corresponding free energy terms, i.e. $\Delta G°(SS_{\mathbf{XX}}/R_{amine})$ and $\Delta G°(RR_{\mathbf{XX}}/R_{amine})$. As observed before, binding of the guest with the absolute configuration opposite to that of the stereocenters of **XX** is invariably preferred. The enantiomeric prefer-

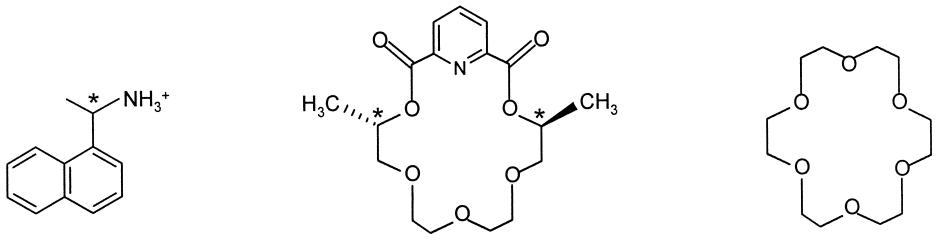

XIX 16 17

Chart 3.

ence of SS_{XX} versus RR_{XX} is expressed by the relevant $\Delta\Delta G° = \Delta G°(SS_{XX}/R_{amine}) - \Delta G°(RR_{XX}/R_{amine})$ terms that amount to 0.3 ± 0.4 (**18**), 0.9 ± 0.2 (**19**), 2.4 ± 0.5 (**20**), and 3.5 ± 0.6 (**21**) KJ mol^{-1}. This trend corroborates the hypothesis that the $\pi-\pi$ stacking interactions between the guest and the host, as well as the steric hindrance to complexation, represent main intrinsic factors for chiral recognition. Another important factor that is entropic in nature may be related to the conformational space available for the most favorable complexation geometry. Molecular modeling points to a facile attainment of the best complexation geometry for the systems in Chart 4, but this may occur at the expense of entropically unfavorable partial locking of methyl rotors and it is probable that the degree to which this occurs differs for the two enantiomers. Indeed, space-filling models of the complexes suggest that partial locking of the methyl rotors is more important for the homochiral complex.

By a similar procedure, protonated cyclodextrin (CD)-amino acid (A) complexes were found to undergo gas-phase ligand exchange by an alkylamine (B) [Eq. (5)] [22]. β-Cyclodextrin (2,3,6-tri-*O*-methyl-β-cyclodextrin) incorporates an amino acid guest in solution to form a complex ($[CD^{\cdot}A^{\cdot}H^{+}]$) that persists when the solution is electrosprayed through a heated capillary into the FTICR analyzer cell containing B = 1-propylamine (**22**) or the racemate of 2-butylamine (**18**)

$$[CD^{\cdot}A^{\cdot}H^{+}] + B \Leftrightarrow [CD^{\cdot}A^{\cdot}H^{+} \cdots B]$$

$$\Leftrightarrow [CD^{\cdot}B^{\cdot}H^{+} \cdots A] \Leftrightarrow [CD^{\cdot}B^{\cdot}H^{+}] + A \qquad (5)$$

The exchange rates were measured and found to differ according to the chirality of A (k_L and k_D in Table 6). Valine is the most reactive and shows the greatest enantioselectivity (k_L/k_D). Similarly, *L*-alanine shows enhanced reactivity relative to the *D*-enantiomer. Phenylalanine behaves unlike the other two

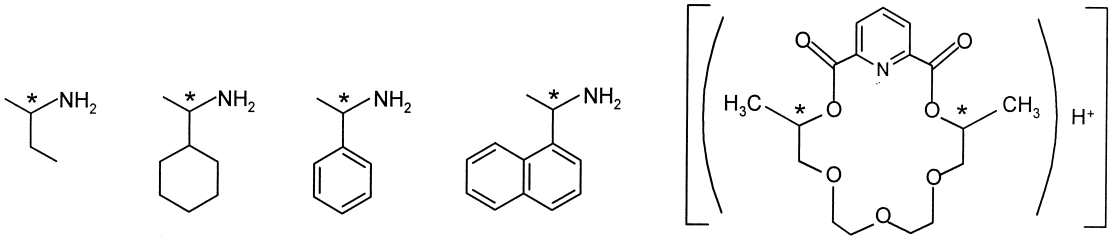

18 19 20 21 XX

Chart 4.

Table 6
Rate constants for chiral guest exchange reactions[a]

Amino acid, A		**22**, B (GB, 217.9)[b]				**18**, B (GB, 220.5)[b]		
	GB[b]	k_L	k_D	k_L/k_D	k_{LD}	k_L	k_D	k_L/k_D
Alanine	213.6	2.4	1.5	1.6	1.9	1.6	1.3	1.2
Valine	215.7	3.1	1.0	3.1	2.0	1.5	1.1	1.4
Phenylalanine	216.6	1.4	1.7	0.8		0.16	0.17	0.9

[a] $k(\times 10^{-11}$ cm^3 molecule^{-1} s^{-1}.
[b] GB, gas-phase basicity (kcal mol^{-1}).

amino acids. It is the least reactive and shows the least enantioselectivity by favoring the *D*-enantiomer, rather than the *L* one. The rate constants k_{LD} of the racemate of alanine and valine are nearly equal to the average of the rate constants k_L and k_D of the pure enantiomers.

The different behavior of phenylalanine, compared to alanine and valine, is attributed to the different structure of the inclusion complex. In fact, whereas alanine and valine are small enough to be completely included in the CD cavity, phenylalanine is so large that only the phenyl side chain is included in the hydrophobic cavity, with the remainder of the amino acid positioned to interact with the hydrophilic rim. The more basic 2-butylamine racemate displays both minor reactivity and enantioselectivity as compared to the less basic 1-propylamine. This suggests that steric interactions are important and, in this case, more important than intrinsic basicity in the guest exchange reaction.

The proton transfer reactions from multiply charged [cytochrome c]$^{+n}$ (n = 7–9) to (*R*)- and (*S*)-2-butylamine (**18** in Chart 4) show a significant enantioselectivity [23]. Ions [cytochrome c]$^{+n}$ (n = 7–9) were produced by ESI and introduced into the analyzer cell of an FTICR containing an alkylamine, i.e. (*R*)- and (*S*)-**18**, 1-propylamine **22**, or *tert*-butylamine **23**. Rate constants for the proton transfer are listed in Table 7.

Proton transfer to (*R*)-**18** is invariably faster than that to (*S*)-**18**, irrespective of the charge state of cytochrome *c*. In any case, the reaction is very inefficient (0.1–0.001%) because of the endoergonicity of the process and the large steric interactions in the corresponding transition structures. The decay of the [cytochrome c]$^{+9}$ ions with reaction time is best represented by a single rate constant, whereas that of the [cytochrome c]$^{+n}$ (n = 7, 8) ions is best represented by two rate constants (fast and slow in Table 7). This is indicative of a single conformer for [cytochrome c]$^{+9}$ and of two conformers for [cytochrome c]$^{+n}$ (n = 7, 8) [24]. The relative amount of these conformers (percent in Table 7) are the same for

Table 7
Rate constants for the proton transfer from [cytochrome c]$^{+n}$ (n = 7–9) to alkylamines[a]

[cytochrome c]$^{+n}$		(*R*)-**18** (GB, 211.7)		(*S*)-**18** (GB, 211.7)		**22** (GB, 210.1)	**23** (GB, 213.0)
n	Type	k_R[b]	Percent	k_S[b]	Percent	k_{22}[b]	k_{23}[b]
9		1.5 ± 0.3 (−11)		2.5 ± 0.2 (−12)		2.2 (−12)	6.1 (−13)
8[c]		2.3 ± 0.5 (−12)		4.6 ± 1.1 (−13)		2.9 (−13)	3.8 (−14)
8	fast	1.0 ± 0.3 (−11)	45	1.9 ± 0.4 (−12)	46	3.1 (−13)	3.7 (−13)
8	slow	1.4 ± 0.1 (−12)	55	3.7 ± 1.0 (−13)	54		
7[c]		2.3 ± 0.1 (−13)		8.4 ± 3.6 (−14)		7.2 (−14)	
7	fast	1.1 ± 0.1 (−11)	21	1.4 ± 0.3 (−12)	30	1.4 (−13)	5.1 (−14)
7	slow	1.3 ± 1.1 (−13)	79	1.4 ± 1.9 (−13)	70		

[a] k's in cm^3 molecule^{-1} s^{-1}.
[b] The figures in parentheses refer to the power of ten. GB, gas-phase basicity (kcal mol^{-1}).
[c] Further reaction of lower-charge daughter species arising from proton transfer.

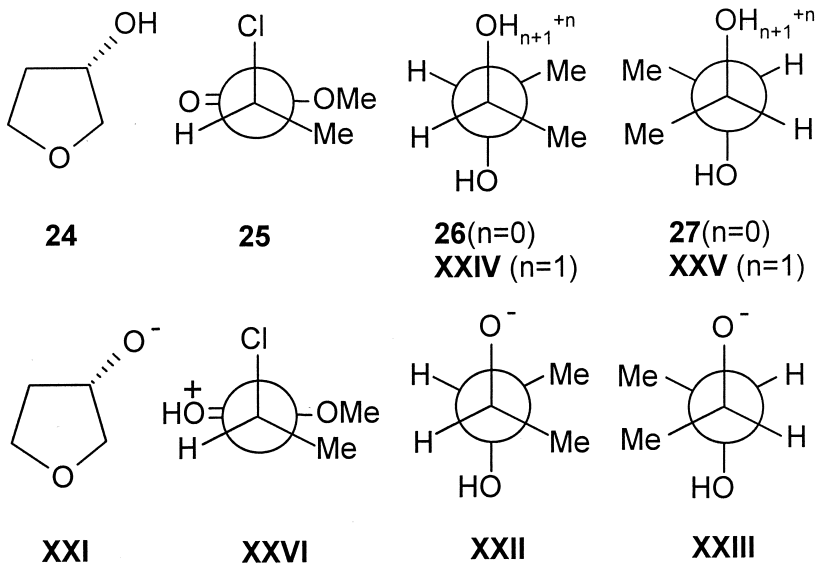

Chart 5.

the *R*- and *S*-enantiomer. (*S*)-**18** exhibits decreasing reactivity with decreasing *n*, as expected from purely Coulombic considerations. In this regard, either **22** or **23** behave in the same manner. With (*R*)-**18**, the rate constant when $n = 9$ and the highest rates when $n = 7, 8$ are approximately equal, suggesting a possible reactive site for the three charged states. A comparison of the rate constants in Table 7 indicates that 1-propylamine **22** is approximately as reactive as (*S*)-**18**, despite the 1.6 kcal mol^{-1} lower basicity. Toward [cytochrome *c*]$^{+n}$ ($n = 8, 9$), *tert*-butylamine **23** is one order of magnitude less reactive than **22**, despite the 2.9 kcal mol^{-1} higher basicity. These findings are interpreted in terms of the strong influential role of steric effects in the highly specific arrangement of the alkylamine toward the multiply charged protein.

3.3. Chiral ion clusters dissociation

The relative stability of diastereomeric complexes between some chiral selectors, such as (*S*)-(+)-3-hydroxy-tetrahydrofuran (**24**) and methyl-(*R*)-(+)-2-chloro-propionate (**25**), and the ions **XXII**–**XXV**, derived from (2*R*, 3*R*)- (**26**) and (2*S*, 3*S*)-2,3-butanediol (**27**) [25], was evaluated by using the kinetic method (Chart 5) [26].

This method is based on the CID of the diastereomeric complexes, e.g. [**XXII**$^{-}$**24**] and [**XXIII**$^{-}$**24**], and the measurement of relative abundances of the corresponding fragment ions, i.e. **XXII** (or **XXIII**) and **XXI**, which reflect the corresponding fragmentation rate constants k_{RR} (or k_{SS}) and $k_{ref'}$ (or $k_{ref''}$) [Eqs. (6a) and (6b)

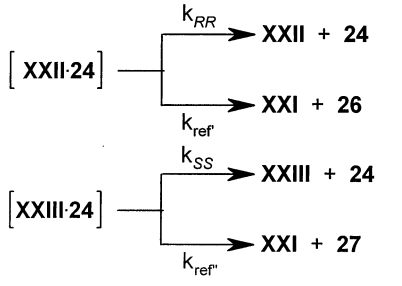

$$\ln\left(\frac{[\mathbf{XXII}]}{[\mathbf{XXI}]}\right)=\ln(k_{RR}/k_{ref'})=\ln K_{eq}^{RR}=-\Delta(\Delta G)^{RR}/RT_{eff} \quad (6a)$$

$$\ln\left(\frac{[\mathbf{XXIII}]}{[\mathbf{XXI}]}\right)=\ln(k_{SS}/k_{ref''})=\ln K_{eq}^{SS}=-\Delta(\Delta G)^{SS}/RT_{eff} \quad (6b)$$

Table 8
Fragment-ion abundance ratios from the CID of diastereomeric complexes

Diastereomeric complex	I_{diol}/I_{ref}	Δ(ΔG) (kcal mol^{-1})	ΔΔ(ΔG) (kcal mol^{-1})
[**XXII** · **24**]	[**XXII**]/[**XXI**] = 12.4	−1.67	0.47
[**XXIII** · **24**]	[**XXIII**]/[**XXI**] = 25.6	−2.14	
[**XXIV** · **25**]	[**XXIV**]/[**XXVI**] = 19.0	−1.94	0.23
[**XXV** · **25**]	[**XXV**]/[**XXVI**] = 26.7	−2.17	

Theoretical treatments [26] lead to the approximate expression in Eqs. (6a) and (6b), where T_{eff} is the effective temperature of the complexes, and the Δ(ΔG)'s are the differences in their dissociation free energies. If the entropy effects of the two competing fragmentation processes cancel, then the Δ(ΔG)'s can be substituted by the Δ(ΔH)'s. This procedure represents a significant source of information on the gas phase acidities, basicities, and proton affinities of a variety of compounds.

The average effective temperature T_{eff}, which is a measure of excess internal energy content per degree of freedom of the ion/molecule complexes, was determined as 333 K from the slopes of the 1/RT dependence of the logarithm of the branching ratios, similar to those of Eqs. (6) involving ions **XXII**–**XXV** and a number of reference molecules. Using this T_{eff} value, the CID results lead to the Δ(ΔG) values reported in Table 8, where I_{diol} represents the abundance of the **XXII**–**XXV** ions from paths k_{RR} and k_{SS} and I_{ref} refers to the abundance of the fragments from paths $k_{ref'}$ and $k_{ref''}$, involving the appropriate chiral selector **24** and **25**.

The differences between the Δ(ΔG) values of diastereomeric complexes [$\Delta\Delta(\Delta G) = \Delta(\Delta G)_{RR} - \Delta(\Delta G)_{SS}$ in Table 8] demonstrate that the kinetic method can be used to enantiodifferentiate chiral ions and molecules in the gas phase.

By the same token, *D*- and *L*-α-amino acids have been enantiodifferentiated in the gas phase based on the kinetics of the CID competitive fragmentation of their Cu(II)-bound trimers [27]. ESI of hydroalcoholic solutions of the amino acid and $CuCl_2$ into the MS source reveals the presence of singly charged, covalently bound cluster ions of type **XXVII** and **XXVIII** (Chart 6). Tetracoordinated trimers **XXVIII** have two weaker, singly bound ligands, that are easily lost by CID. This feature provides the basis for efficient chiral distinction.

The gas-phase chiral discrimination of six amino acids by Cu(II) complexation have been investigated and their behavior contrasted with the chiral effects observed in ligand exchange chromatography (LEC) [28]. In all instances, $\mathbf{XXVII}_{(L\text{-Pro},L\text{-Pro})}$ was used as the reference adduct. The CID results are given in Table 9.

A good correlation is observed between the chiral resolution factors (CRF), taken as the ratios between the fragment–ion abundances of the hetero- (*D*) and the homochiral (*L*) trimers relative to that of the reference adduct, and the LEC selectivity values α. It is concluded that the interactions between ligands,

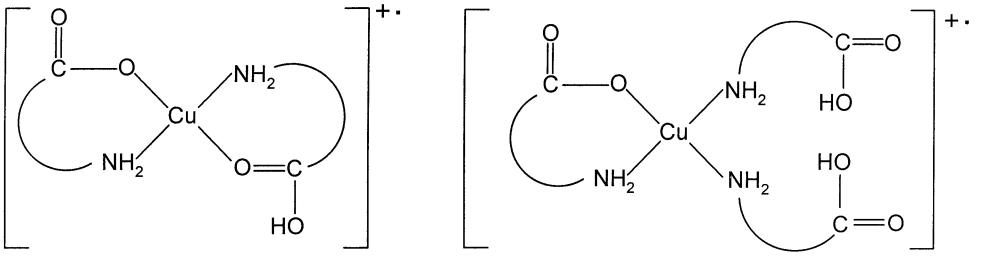

XXVII **XXVIII**

Chart 6.

Table 9
Fragment-ion abundance ratios from the CID of Cu(II)-bound trimeric cluster ions

Amino acid, A	**XXVII**$_{(L\text{-Pro,A})}$/ **XXVII**$_{(L\text{-Pro},L\text{-Pro})}$ [a]	R[b]	α[c]	ΔCu(II)′ (KJ mol^{-1})[d]
Tyr	43 (*D*); 4.7 (*L*)	9.2	3.1	6.5
Leu	0.099 (*D*); 0.11 (*L*)	0.87	1.0	−0.41
Met	60 (*D*); 33 (*L*)	1.8	1.15	1.7
Phe	16 (*D*); 2.1 (*L*)	7.4	2.9	5.8
Thr	0.89 (*D*); 0.88 (*L*)	1.0	1.75	0.029
Asp	4.5 (*D*); 3.2 (*L*)	1.4	1.3	1.0

[a] Abundance ratios for the heterochiral (*D*) and the homochiral (*L*) cluster ions.
[b] Chiral resolution factor, *R*, as the ratio between the heterochiral (*D*) and the homochiral (*L*) abundance ratios.
[c] LEC selectivity values.
[d] See text, T_{eff} = 350 K.

which determine chiral discrimination, are similar in solution and in the gas phase.

The degree of chiral discrimination is defined from the relative copper(II) affinity $\Delta Cu(II)' = \Delta Cu(II)_{(D)} - \Delta Cu(II)_{(L)} = RT_{eff}\ \ln(CRF)$, with $\Delta Cu(II) = \ln(\mathbf{XXVII}_{(L\text{-Pro,A})}/\mathbf{XXVII}_{(L\text{-Pro},L\text{-Pro})})$. The $\Delta Cu(II)'$ terms in Table 9 indicate that the heterochiral complexes of aromatic amino acids, i.e. tyrosine and phenylalanine, are significantly more stable than the homochiral analogs. The same is true, although to a lesser extent, for the complexes with methionine and aspartic acid. The heterochiral complex with leucine is instead slightly less stable than the homochiral form. Finally, there is no significant stability difference between the diastereomeric complexes with threonine.

The kinetic method has been applied to the enantiodifferentiation of chiral amino acids A through the measurement of the relative stability of their homo- and heterochiral proton-bound complexes with a chiral selector C [29]. The stability of proton-bound adducts $[ACH^+]$ can be evaluated from CID of the proton-bound three-body adducts $[A_2CH^+]$. The $[ACH^+]/[A_2H^+]$ ratio is used [Eq. (7)]

$$[A_2CH^+] \rightarrow [A_2H^+] + C \qquad (k_{A2}) \qquad (7a)$$

$$[A_2CH^+] \rightarrow [CH^+] + A_2 \qquad (k_C) \qquad (7b)$$

$$[A_2CH^+] \rightarrow [ACH^+] + A$$

$$\text{(doubly degenerate)} \quad (k_{AC}) \qquad (7c)$$

$$[A_2CH^+] \rightarrow [AH^+] + AC$$

$$\text{(doubly degenerate)} \quad (k_A) \qquad (7d)$$

The relative gas phase basicities (GB) of the molecular pairs AC and A_2 can be derived from Eqs. (8) and (9)

$$\ln([A_2H^+]/[CH^+]) = \ln(k_{A2}/k_C) = \{GB(A_2) - GB(C)\}/RT_{eff} \qquad (8)$$

$$\ln(\{[ACH^+]/2\}/[A_2H^+]) = \ln(\{k_{AC}/2\}/k_{A2}) = \{GB(AC) - GB(A_2)\}/RT_{eff} \qquad (9)$$

The chiral discrimination factor, ΔR^{chiral}, is defined by Eq. (10)

$$\Delta R^{chiral} = \{[ACH^+]_{hetero}/[A_2H^+]\}/\{[ACH^+]_{homo}/[A_2H^+]\} = \{\{[ACH^+]/[A_2H^+]\}_{DL} + \{[ACH^+]/[A_2H^+]\}_{LD}\}/\{\{[ACH^+]/[A_2H^+]\}_{DD} + \{[ACH^+]/[A_2H^+]\}_{LL}\} \qquad (10)$$

The $[ACH^+]/[A_2H^+]$ ratios from CID of various mixtures of chiral amino acids are reported in Table 10.

Using Eqs. (9) and (10), the relative GB (ΔGB^{chiral}) of the hetero- versus homochiral proton-bound complexes can be expressed as in Eq. (11)

$$\Delta GB^{chiral} = GB(AC_{hetero}) - GB(AC_{homo}) = RT_{eff}\ \ln\{\Delta R^{chiral}\} \qquad (11)$$

The relevant ΔGB^{chiral} values, calculated by using T_{eff} = 970 K [30], are listed in Table 10. According to the reported values, the heterochiral TrpPro and PheAla complexes are more stable than the homochiral ones. The reverse is true for the PhePro and PheVal complexes. The stereochemistry associated with the CID of diastereomeric peptides has been investigated using a similar approach. The results suggest that the secondary structure of protonated peptides may play an important role in their gas-phase behavior [31].

Table 10
Fragment-ion abundance ratios from the CID of proton-bound A_2CH^+ clusters

Amino acid, A	Selector, C	$[ACH^+]/[A_2H^+]$	ΔR^{chiral}	SD[a] of ΔR^{chiral}	ΔGB^{chiral} (KJ mol^{-1})[b]
Trp	Pro	1.528 (*DD*); 1.529 (*LL*); 1.656 (*DL*); 1.643 (*LD*)	1.079	0.004	0.6
Pro	Trp	2.936 (*DD*); 3.049 (*LL*); 3.429 (*DL*); 3.461 (*LD*)	1.151	0.008	1.1
Phe	Ala	0.291 (*DD*); 0.291 (*LL*); 0.315 (*DL*); 0.313 (*LD*)	1.079	0.008	0.6
Phe	Pro	15.221 (*DD*); 15.098 (*LL*); 9.346 (*DL*); 9.901 (*LD*)	0.645	0.015	−3.3
Phe	Val	0.786 (*DD*); 0.776 (*LL*); 0.744 (*DL*); 0.749 (*LD*)	0.956	0.004	−0.4

[a] SD = standard deviation.
[b] Positive values indicate higher basicity for the heterochiral complex.

4. Chiral recognition in supersonically expanded molecular complexes

Molecular complexes represent the simplest model systems for studying the physical and chemical properties of molecules in the transition from the gas phase to the condensed phase. They are ideal systems for disentangling the intrinsic structural factors affecting molecular reactivity from solvation effects and for gathering information on the sensitivity of molecular stability to microsolvation. An assessment of the structure of molecular complexes and a microscopic understanding of their intracomplex forces requires spectroscopic investigation in the isolated state. Recent progress in this area was stimulated by the introduction of new experimental methodologies as well as by the growing interest in these systems as models for understanding enantioselectivity in chemistry and biology. Supersonic beams allow the synthesis of otherwise fragile molecular complexes in quantities suitable for their spectroscopic characterization. Laser sources and synchroton radiation allow precise evaluation of their energetics, dynamics, and structure.

The following sections will focus on the structure and energetics of chiral molecular complexes studied with resonance-enhanced multiphoton ionization (REMPI), laser induced fluorescence (LIF), and hole burning (HB) spectroscopy. For detailed information on these spectroscopic methodologies as well as on the techniques for the production and the separation of molecular complexes in supersonic beams, the reader is referred to the excellent reviews by Brutschy [32] and Neusser and Krause [33].

4.1. Structure of supersonically expanded molecular complexes

Supersonic expansion of a carrier gas, typically helium or argon, seeded with molecules with many degrees of freedom may result in the production of weakly bound molecular complexes in their electronic ground state S_0 with translational and vibrational temperatures of a few kelvins. Different conformers corresponding to different local minima of the potential energy surface can coexist in the cold region of the jet. If separated by significant energy barriers, these forms are relatively stable and can be probed by LIF and REMPI spectroscopies. Because of the low internal temperature of the probed complexes, their LIF and REMPI spectra are generally very sharp and well resolved. The LIF method combines the formation of a molecular complex containing a fluorescent moiety (F) by supersonic expansion and the measurement of the laser-induced emitted fluorescence. The F molecule is laser excited to the fluorescent S_1 state. The emitted fluorescence is collected at right angles to both the excitation laser pulse and the beam axis and recorded. The fluorescence decay times are measured with a photomultiplier (Fig. 3).

Relative to the excitation spectrum of the bare F ($h\nu$), complexation usually results in the appearance of new spectral features ($h\nu'$) falling at different wavelengths (microscopic solvent shift $\Delta\nu = h\nu' - h\nu$). The shift may be toward the red (negative $\Delta\nu$ value) or toward the blue (positive $\Delta\nu$ value). A red shift indicates a decrease of the $S_1 \leftarrow S_0$ energy gap in the [F˙ solv] complex relative to the bare F, whereas a blue shift indicates the opposite. In general, diaste-

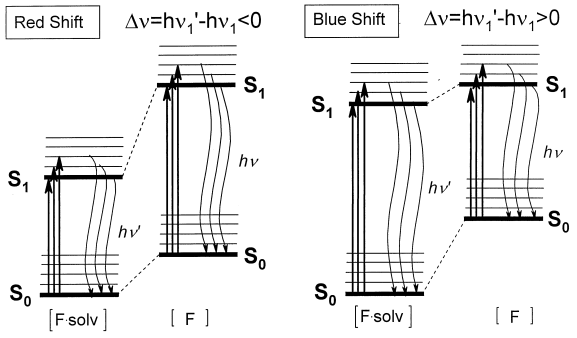

Fig. 3. Schematic representation of the ground and first excited levels of the bare chromophore F and of its complex with a solvent molecule solv: $h\nu$ = fluorescence photon of bare F; $h\nu'$ = fluorescence photon of its complex with solv; $\Delta\nu = h\nu' - h\nu$ = microscopic solvent shift.

reomeric pairs from complexation of a chiral solv with chiral F are characterized by the nonequivalence of their interaction energy in both the ground and the excited states and, therefore, are expected to exhibit different microscopic solvent shifts $\Delta\nu$. Besides, complexation normally results in a drastic variation of the fluorescence lifetime τ of the chromophore due to change of the radiative lifetime or a decrease of the intersystem-crossing rate constant. This is the basis of the LIF application to chiral recognition in the isolated state.

The LIF spectral shifts $\Delta\nu$ and the fluorescence lifetimes τ concerning the complexes between (*R*)-2-naphthyl-1-ethanol, as the fluorescent chromophore F, and a variety of primary and secondary aliphatic alcohols (solv) are listed in Table 11 [34].

In general, the excitation spectra of these complexes show intense features, accompanied by smaller signals placed at the low energy side. These signals are mainly due to several conformational isomers of the 1:1 complexes, as further demonstrated by HB experiments [34(c)]. The origin bands of the complexes with primary and secondary alcohols are red shifted with respect to that of bare F. This suggests that the major contribution to the intracomplex forces is due to hydrogen bonding between solv and F, with the latter acting as the hydrogen donor. In fact, when the hydrogen donor is solv, as in the case of the acidic trifluoroethanol, a blue shift is observed. Similar

Table 11
Main solvent shifts ($\Delta\nu$) and fluorescence lifetimes (τ) of [F · solv] complexes [F = (*R*)-2-naphthyl-1-ethanol]

solv	$\Delta\nu$ (cm^{-1}) [τ (ns) in parentheses]
None	0 (45), +39 (35), +76 (20), +278, +339, +434
Methanol	−67 (33), −55 (160), −43 (151)
Ethanol	−61 (63), −55, −52 (126)
Trifluoroethanol	+24 (84), +51 (158)
1-Propanol	−138 (119), −112 (54), −60 (55), −55 (119)
1-Butanol	−158 (112), −144, −125, −71 (125)
(*S*)-2-butanol	−136, −114, −73, −28, +6
(*R*)-2-butanol	−125, −87, −69, +29
(*S*)-2-pentanol	−147, −133, −119, −52, +50
(*R*)-2-pentanol	−85, −54
(*S*)-2-hexanol	−127, −110, +53
(*R*)-2-hexanol	−106, −73, −65
(*S*)-2-octanol	−160, −151, −142, −135, −17
(*R*)-2-octanol	−133, −122, −115, −107, −91, −79, −63, −38
(*S*)-2-methyl-1-butanol	−84 (135), −51, −34, −19
(*R*)-2-methyl-1-butanol	−134 (140), −118, −62 (123), +54

spectra are observed for the diastereomeric complexes with chiral 2-methyl-1-butanols. However, the band origin of the heterochiral complex falls 50 cm^{-1} toward the blue relative to that of the homochiral adduct. The trend is fully reversed for the complexes with chiral secondary alcohols. In this case, it is the heterochiral complexes that exhibit larger red shifts.

The most intense bands observed in the excitation spectra of the complexes often exhibit a decay time τ longer than that of bare F. However, some exceptions are observed and τ does not decrease monotonically with the interaction energy, as could be expected. The τ variations can be instead associated with the effect of complexation on the photophysics of the chromophore. Thus, no clear-cut relationship can be established between τ and the structure and configuration of solv. Nonetheless, because of the peculiar sensitivity of the excited state dynamics to the subtle perturbation induced by complexation, the decay time τ can be seen as a phenomenological tool for enantiodifferentiating chiral molecules in the isolated state.

A more detailed structural characterization of su-

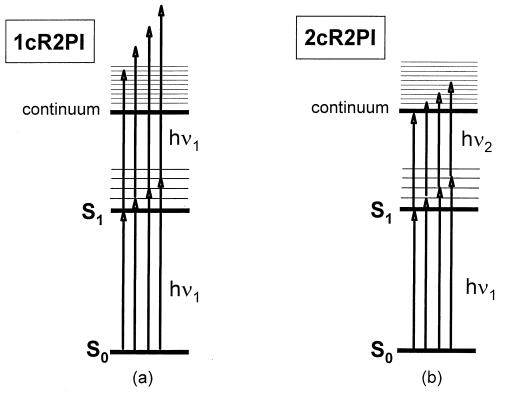

Fig. 4. Schematic representation of the (a) 1cR2PI and (b) 2cR2PI experiments. The 1cR2PI spectra are obtained by exciting the species of interest to the S_1 excited state by absorption of one photon of frequency ν_1 and by ionizing it by absorption of another photon with the same frequency ν_1. The 2cR2PI excitation spectra are obtained by fixing ν_2 at a value slightly above the ionization threshold and by scanning ν_1.

personically expanded molecular complexes is obtained using the REMPI spectroscopy [35]. The supersonically expanded species under investigation is ionized through absorption of several laser photons of adequate energy and mass selected by a time-of-flight (TOF) mass spectrometer. The species of interest is ionized through an R2PI process, i.e. one photon, ν_1, is used to excite the species from its ground state S_0 to its first electronically excited state S_1 and a second photon from the same laser beam (one-color R2PI or 1cR2PI) or from another tuned at a different frequency, ν_2 (two-color R2PI or 2cR2PI), leads it to the continuum (Fig. 4).

The ν_1 wavenumber dependence of a given mass resolved ion represents the absorption spectrum of the species and contains important information about its electronic excited state S_1. In the 1cR2PI experiments on supersonically expanded clusters, some excess energy may be imparted to high-order complexes present in the beam, which may partially decompose, yielding the same ionic fragments arising from the 1:1 adduct [Fig. 4(a)]. These spurious signals usually complicate the interpretation of the spectrum of the 1:1 complex. This drawback is absent in the 2cR2PI experiments [Fig. 4(b)] because, in this case, no significant excess energy is imparted to the complexes and decomposition of conceivable high-order clusters is strongly depressed.

The mass resolved 1cR2PI spectrum of the bare chiral chromophore R, i.e. (*R*)-(+)-1-phenyl-1-propanol, shows three intense signals at 37 577 (A), 37 618 (B), and 37 624 cm^{-1} (C) in the electronic $S_1 \leftarrow S_0$ band origin region. A similar triplet falls at 38 106, 38 148, and 38 155 cm^{-1}. This pattern is common to substituted arenes and is interpreted as due to three stable conformers. Quantum chemical calculations at the RHF/3-21G and B3LYP/6-31G levels of theory confirm this hypothesis.

In qualitative agreement with the previous LIF results, the R2PI absorption spectra of the complexes between the chromophore R and a variety of primary and secondary alcohols and amines exhibit major characteristic peaks (α and β in Fig. 5) that somewhat reproduce the pattern of the bare chromophore but shifted toward the red or the blue by an extent denoted as $\Delta\nu_\alpha$ and $\Delta\nu_\beta$, respectively (Table 12).

The $\Delta\nu_\alpha$ and $\Delta\nu_\beta$ shifts from the complexes with primary alcohols are linearly correlated to the proton affinity (PA) of primary solv [PA(solv; kcal mol^{-1}) = (180 ± 0.6) − (0.076 ± 0.006)$\Delta\nu(cm^{-1})$; $r^2 = 0.951$], that in turn determines the strength of the O–H · · · O hydrogen bond between the R donor and the solv acceptor (Fig. 6).

These features allow one to assign the α and β spectral signatures of Fig. 5 to two different sets of [R· solv] complexes, where R is in a given conformation and acts as the hydrogen-bond donor to solv and where the alkyl group of solv maintains a specific spatial orientation toward the aromatic ring of R. In this case, both the electrostatic and the dispersive (polarization, charge exchange, etc.) interactions cooperate in stabilizing the adducts in the ground and excited states.

According to Fig. 6, the signals of the complexes with secondary alcohols and amines display $\Delta\nu$ values that are less negative than expected on the grounds of the linear correlation obtained for the primary alcohols. These deviations suggest that the relative contributions of electrostatic and dispersive forces in these systems are substantially different from those

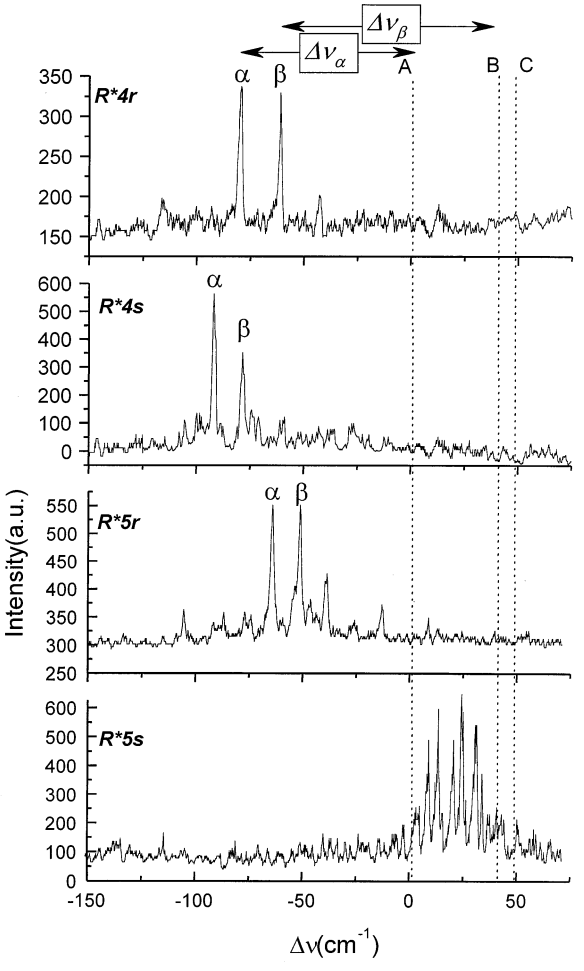

Fig. 5. 2cR2PI excitation spectra of the complexes between R and 2-alkanols, measured at their *m/z* values and at a total stagnation pressure of 4×10^5 Pa.

operating in the corresponding complexes with primary alcohols.

Comparison of the $\Delta\nu$ values of diastereomeric complexes with 2-butanols, 2-pentanols, and 2-butylamines indicates that the relative extent of electrostatic and dispersive forces depends upon the nature, the bulkiness, and the configuration of solv. The $\Delta(\Delta\nu_\alpha) = [(\Delta\nu_\alpha)_{\text{homo}} - (\Delta\nu_\alpha)_{\text{hetero}}] = +13 \quad \text{cm}^{-1}$ difference between the red shifts of the homochiral and the heterochiral complexes with 2-butanols finds a close analogy with the LIF red-shift difference of the corresponding adducts with (*R*)-(+)-2-naphthyl-1-ethanol F (Table 11) [34]. However, whereas the LIF results from the diastereomeric [F·2-pentanol] complexes are qualitatively similar to those with the other 2-alkanols, the homochiral and the heterochiral [R·2-pentanol] complexes display a negative spectral shift difference [$\Delta(\Delta\nu_\alpha) = \sim -89$ cm^{-1}], in striking contrast to the positive one observed for the [R·2-butanol] pair. This marked spectral diversity can be attributed to the shorter side chain and the wider "π-electron bed" of F, relative to R, that allows the establishment of a synergy between attractive electrostatic and dispersive forces in [F·2-pentanol] in both the S_0 and S_1 states. In the [R·2-pentanol] complexes, a similar cooperation is hindered by the greater steric congestion because of the relatively bulky side chain and relatively narrow π system of the chromophore. This is particularly evident in the heterochiral complex with (*S*)-2-pentanol, whose blue shift is rationalized in terms of a predominant O–H $\cdots$ π electrostatic interaction (or even a change in the nature of the hydrogen-bond donor) determined by its high steric congestion. Indeed, a similar blue shift is observed in the 1cR2PI absorption spectrum of the 1:1 cluster

Table 12
R2PI band shifts relative to jet-cooled 1:1 complexes between (*R*)-(+)-1-phenyl-1-propanol and primary and secondary alcohols (solv)

Mode	solv	$\Delta\nu_\alpha$ (cm^{-1})[a]	$\Delta\nu_\beta$ (cm^{-1})[b]	PA (kcal mol^{-1})[c]
1cR2PI	methanol	−2	−6	180.3
1cR2PI	ethanol	−78	−63	185.6
1cR2PI	1-propanol	−90		188.0
2cR2PI	1-butanol	−96	−101	188.6
1cR2PI	1-pentanol	−118	−136	*189.2*
2cR2PI	2-propanol	−87	−71	189.5
1cR2PI	3-pentanol	−108		*195.6*
2cR2PI	(*R*)-2-butanol	−79	−102	195.0
2cR2PI	(*S*)-2-butanol	−92	−119	195.0
2cR2PI	(*R*)-2-pentanol	−64	−92	*195.6*
2cR2PI	(*S*)-2-pentanol	∼+25		*195.6*
1cR2PI	(*R*)-2-butylamine	−109		222.2
1cR2PI	(*S*)-2-butylamine	−127		222.2

[a] Band shifts of the α peaks, relative to the band origin A of bare R.
[b] Band shifts of the β peaks, relative to the band origin B of bare R.
[c] See [38]. Values in italic estimated from the PA limits of primary and secondary alcohols [39], using the group additivity method [40].

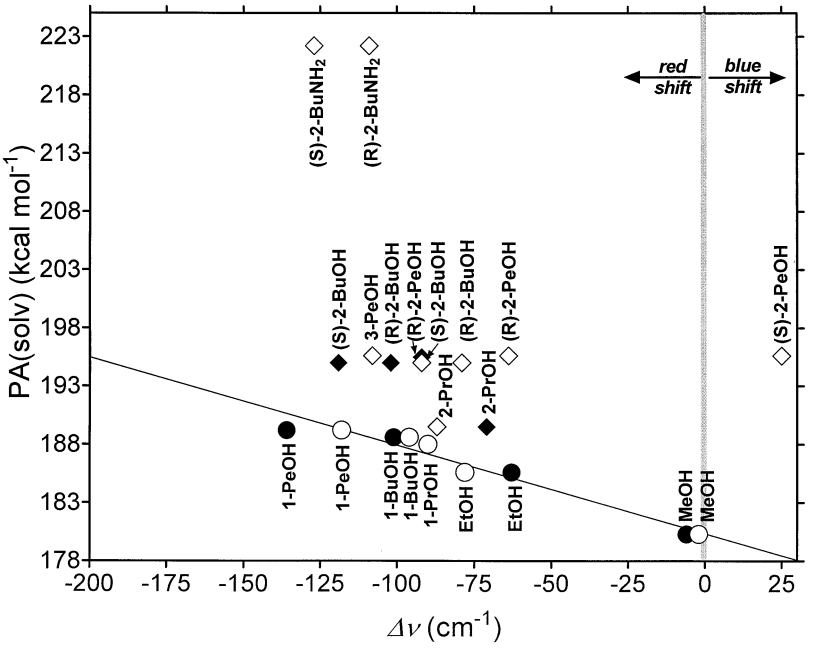

Fig. 6. Diagram of the band origin shifts $\Delta\nu$ of the molecular complexes between R and primary and secondary alcohols and amines. The circles refer to primary alcohols (open circles = $\Delta\nu_\alpha$; filled circles = $\Delta\nu_\beta$); the diamonds refer to secondary alcohols and amines (open diamonds = $\Delta\nu_\alpha$; filled diamonds = $\Delta\nu_\beta$).

between R and water, where the solvent can establish, with the aromatic ring of the chromophore, only electrostatic O–H $\cdots$ π interactions [36].

4.2. Energetics of supersonically expanded molecular complexes

Further insights into the forces operating in the molecular complexes between R and 2-alkanols are obtained from the measurement of their binding energies [37]. The procedure used is summarized in Fig. 7.

The binding energy D_0'' of a molecular complex is derived from the difference between its dissociative ionization threshold ($h\nu_1' + h\nu_3'$) and the ionization threshold of bare R ($h\nu_1 + h\nu_2$). The binding energy D_0' of the molecular complexes in the S_1 excited state is taken to be equal to $D_0'' - \Delta\nu$, using the appropriate $\Delta\nu$ terms in Table 12. The dissociation energy D_0^+ of the ionic cluster is obtained from the difference between its dissociative ionization threshold ($h\nu_1' + h\nu_3'$) and its ionization threshold ($h\nu_1' + h\nu_2'$).

The 2cR2PI ionization thresholds correspond to the signal onset of the relevant ionic fragment obtained by scanning photon ν_2 while keeping ν_1 at the fixed value corresponding to the $S_1 \leftarrow S_0$ transition (Fig. 8). The relevant results are listed in Table 13.

The D_0'' value of the complex between R and 1-butanol (2.6 $\pm$ 0.2 kcal mol^{-1}) conforms well to the approximate value of 2–3 kcal mol^{-1} indirectly estimated for the dissociation energy of the complex between (*R*)-(+)-2-naphthyl-1-ethanol F and methanol [34(b)]. Concerning the diastereomeric complexes, the homochiral adducts are invariably more stable than the heterochiral ones. This trend extends to the corresponding S_1 excited complexes as well. This observation, coupled with the appreciable deviation from linearity of the corresponding $\Delta\nu$ values (Fig. 6), corroborates the view that the interaction forces in these complexes are affected by steric congestion to a different extent.

Their sensitivity to steric factors is demonstrated by the diverging observations that (Table 13): (1) in

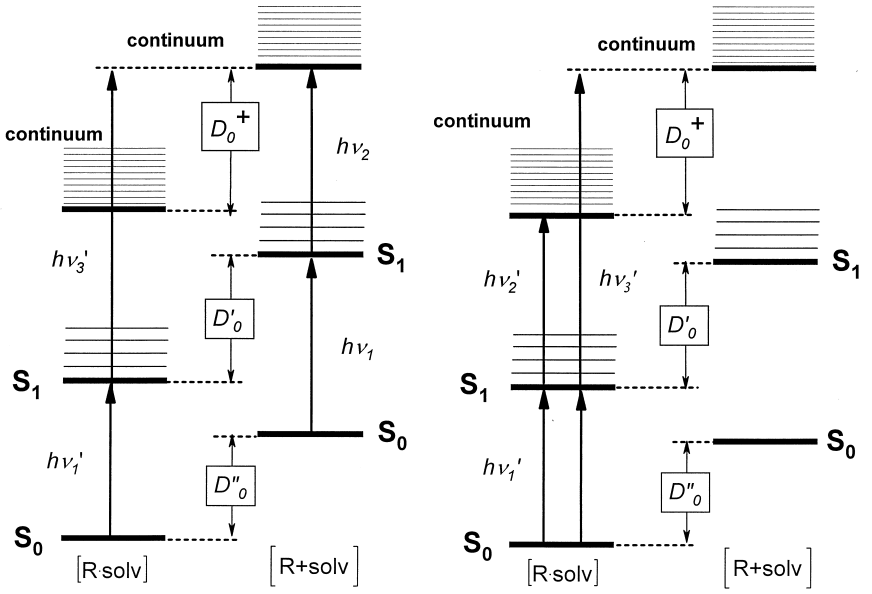

Fig. 7. Schematic representation of the energy levels of the bare R (R + solv) and of its complexes with solv (R · solv). D''_0, D'_0, and D_0^+ are the binding energies of the adducts in the ground, excited, and ionized state, respectively.

the diastereomeric pair with 2-butanols, the larger red shift is associated with the less stable heterochiral complex, (2) in the diastereomeric pair with 2-pentanols, the less stable heterochiral complex exhibits a blue shift and the most stable homochiral complex exhibits a red shift. This implies that the relatively high steric congestion (making the heterochiral complex with (*S*)-2-butanol less stable than the homochiral analog) is insufficient to alter significantly the nature of the attractive intracomplex forces. This is no longer true in going from the homochiral complex with (*R*)-2-butanol to the homochiral complex with (*R*)-2-pentanol. In fact, steric congestion in the latter complex is so high as to modify to some extent the nature of the attractive intracomplex forces and, therefore, the magnitude of its binding energy in both the ground and the excited states relative to those operating in the homologous complex with (*R*)-2-butanol. This trend goes to extremes in the least stable heterochiral adduct with (*S*)-2-pentanol. The low binding energy of this complex and the blue shift accompanying its $S_1 \leftarrow S_0$ transition point to an

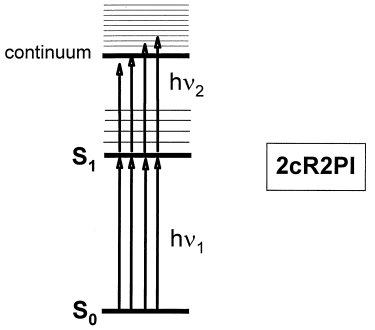

Fig. 8. Schematic representation of the procedure for the measurement of the ionization thresholds by 2cR2PI experiments.

Table 13
Spectral shifts ($\Delta\nu$) and binding energies [D''_0, D'_0, and D_0^+ (see text)] of the molecular complexes between R and some alcohols (solv) (1 kcal mol^{-1} = 349.77 cm^{-1})

solv	$\Delta\nu$ (cm^{-1})	D''_0 (kcal mol^{-1})	D'_0 (kcal mol^{-1})	D_0^+ (kcal mol^{-1})
Water	+88 ± 2	4.8 ± 0.2	4.6 ± 0.2	5.4 ± 0.2
2-Propanol	−87 ± 2	3.7 ± 0.2	3.9 ± 0.2	
1-Butanol	−96 ± 2	2.6 ± 0.2	2.9 ± 0.2	6.5 ± 0.2
(*S*)-2-butanol	−92 ± 2	4.8 ± 0.2	5.1 ± 0.2	6.8 ± 0.2
(*R*)-2-butanol	−79 ± 2	5.9 ± 0.2	6.1 ± 0.2	8.4 ± 0.2
(*S*)-2-pentanol	+25 ± 2	3.1 ± 0.2	3.1 ± 0.2	4.6 ± 0.2
(*S*)-2-pentanol	−64 ± 2	4.7 ± 0.2	4.9 ± 0.2	8.5 ± 0.2

exceedingly high steric congestion, which dramatically perturbs the spatial arrangement of the two moieties so as to allow only attractive O–H $\cdots$ π-ring electrostatic forces, rather than dispersive interactions.

Inspection of the data in Table 13 reveals that the D_0^+ values always exceed the corresponding D''_0 interaction energies. The slow rise of the ion current observed in the 2cR2PI spectra suggests a significant geometry change of the complex in its excited and ionic state and, therefore, the phenomenological D_0^+ terms of Table 13 are probably not representative of the actual binding energies of the ionized molecular complexes. Nevertheless, they provide an additional phenomenological tool for chiral recognition in the isolated state. Indeed, the relatively high D_0^+ values of the homochiral adducts (Table 13) are mirrored by less extensive fragmentation observed in the corresponding 1cR2PI/TOF mass spectra (Fig. 9).

5. Conclusions and prospects

Noncovalent interactions constitute the basis for information transfer between molecules in living systems as well as in synthetic supramolecular structures. Despite an ever more accurate description of biological systems and their modeling by synthetic host/guest complexes, a systematic and general understanding of the underlying intermolecular forces is still in its infancy. A major problem is presented by the unpredictable action of the solvent, which mitigates specific intermolecular interactions, fundamental in biological and supramolecular host/guest aggregates, so as to make entropy terms sometimes predominant.

The advantages connected with studying enantioselectivity in simple complexes in the gas phase instead of in complicated associations in solution arise from the possibility to make precise statements upon the nature and structure of the complexes and to determine with great accuracy their relative stability and reactivity in the absence of any perturbing environmental effects. The above array of gas-phase studies on kinetic and thermodynamic enantioselectivity in ionic and neutral complexes represents a first attempt to provide some positive pieces of information on intrinsic noncovalent interactions governing chiral discrimination.

An important, but often ignored requisite for evaluating enantioselectivity in the gas phase, concerns the retention of the original configuration of the chiral partners after complexation. This aspect becomes crucial in the MS investigation of ion/molecule aggregates owing to the pronounced electrostatic interactions developed in the complexation and the high propensity of charged moieties to rearrange. In this respect, the results of a comprehensive radiolytic investigation on the kinetics and mechanisms of the gas-phase rearrangement of chiral intermediates involved in most classical ion/molecule reactions provide some clues about the lack of chiral discrimination observed in some MS analyses of diastereomeric ion/molecule complexes and allow identification of generalizable parameters that can be manipulated for removing such a failure.

Quantitative measurements of gas-phase enantioselectivity by MS require approaches adequate for identifying the intracomplex forces governing chiral ion/molecule associations and ligand exchange reactions. The presented FTICR and CID results demonstrate that chiral discrimination in gas-phase ion/molecule reactions is mainly determined by short-range forces and by steric hindrance in the relevant collision complexes and that these intrinsic interactions are dramatically affected by solvation. Another important factor, which is entropic in nature, is related to the conformational space available to complexation.

Finally, tackling gas-phase enantioselectivity problems with spectroscopic methodologies (such as REMPI-TOF) originally designed for classical chemical physics studies allows definition of the structure and relative stability of supersonically expanded neutral diastereomeric aggregates, otherwise unstable under normal conditions, in both their ground and electronically excited states and determination of the short-range forces responsible for their behavior.

There is no doubt that a more quantitative application of sophisticated spectroscopic methodologies in the field of gas-phase chiral discrimination and the

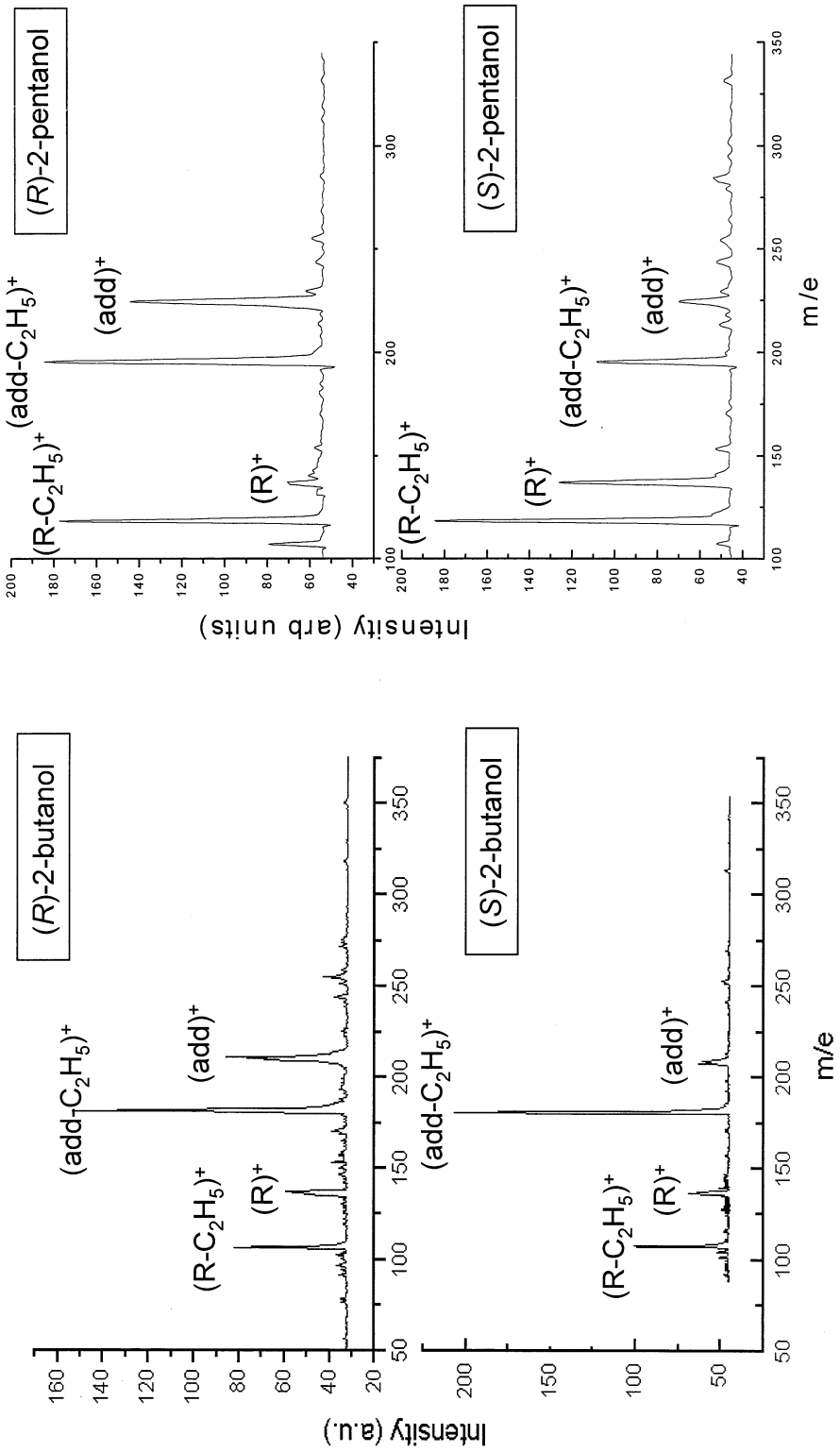

Fig. 9. 1cR2PI-TOF spectra of diastereomeric complexes between R and 2-butanols and 2-pentanols (add = adduct).

development of novel tools for the vaporization of nonvolatile chiral compounds will lead in the near future to a deeper comprehension of the basic principles governing gas-phase enantioselectivity and of those cooperative intracomplex interactions that control the transfer of chemical information between molecules in living systems and which constitute the basis of millions of years of natural evolution.

Acknowledgements

This work was supported by the Italian Ministero della Università e della Ricerca Scientifica e Tecnologica (MURST) and by the Consiglio Nazionale delle Ricerche (CNR).

References

[1] H.J. Schneider, Angew. Chem. Int. Ed. Engl. 30 (1991) 1417.
[2] (a) M. Sawada, Biological Mass Spectrometry: Present and Future, T. Matsuo, R.M. Caprioli, M.L. Gross, Y. Seyama (Eds.), Wiley, New York, 1994, Chap. 3.19, p. 639; (b) M. Sawada, Mass Spectrom. Rev. 16 (1997) 73.
[3] (a) H.M. Fales, G.J. Wright, J. Am. Chem. Soc. 99 (1977) 2339; (b) F.J. Winkler, D. Stahl, F. Maquin, Tetrahedron Lett. 27 (1986) 335; (c) F.J. Winkler, R. Medina, J. Winkler, H. Krause, J. Chromatogr. A 666 (1994) 549; (d) F.J. Winkler, R. Medina, J. Winkler, H. Krause, J. Mass Spectrom. 32 (1997) 1072.
[4] (a) H. Suming, C. Yaozu, J. Longfei, X. Shuman, Org. Mass Spectrom. 21 (1986) 7; (b) N.M. Sellier, C.T. Bouillet, D.L. Douay, J.C.E. Tabet, Rapid Commun. Mass Spectrom. 8 (1994) 891.
[5] E.N. Nikolaev, G.T. Goginashvili, V.L. Tal'rose, R.G. Kostyanovsky, Int. J. Mass Spectrom. Ion Processes 86 (1988) 249. See also: (a) E.N. Nikolaev, T.B. McMahon, Proceedings of the 43rd Annual Conference on Mass Spectrometry and Allied Topics, Atlanta, Georgia, 1995, p. 973; (b) E.N. Nikolaev, E.V. Denisov, Proceedings of the 44th Annual Conference on Mass Spectrometry and Allied Topics, Portland, Oregon, 1996, p. 415.
[6] M. Speranza, Fundamentals and Applications of Gas Phase Ion Chemistry, K.R. Jennings (Ed.), Kluwer Academic, Dordrecht, The Netherlands, 1999, p. 335, and references therein.
[7] See, for instance: (a) F.G. Bordwell, Acc. Chem. Res. 3 (1970) 281; (b) R.M. Magid, Tetrahedron 36 (1980) 1901; (c) F. Carrion, M.J.S. Dewar, J. Am. Chem. Soc. 106 (1984) 3531; (d) R.D. Bach, G.J. Wolber, J. Am. Chem. Soc. 107 (1985) 1352; (e) Y.S. Park, C.K. Kim, B.S. Lee, I. Lee, J. Phys. Chem. 99 (1995) 13 103; (f) T. Borrmann, W.D. Storher, Liebigs Ann. (1996) 1593.
[8] (a) E. Dezi, A. Lombardozzi, A. Pizzabiocca, G. Renzi, M. Speranza, J. Chem. Soc. Chem. Commun. (1995) 547; (b) G. Renzi, A. Lombardozzi, E. Dezi, A. Pizzabiocca, M. Speranza, Chem. Eur. J. 2 (1996) 316; (c) E. Dezi, A. Lombardozzi, G. Renzi, A. Pizzabiocca, M. Speranza, Chem. Eur. J. 2 (1996) 323.
[9] A. Troiani, F. Gasparrini, F. Grandinetti, M. Speranza, J. Am. Chem. Soc. 119 (1997) 4525.
[10] A. Troiani, M. Speranza, J. Org. Chem. 63 (1998) 1012.
[11] M. Speranza, A. Troiani, J. Org. Chem. 63 (1998) 1020.
[12] (a) P. Crotti, F. Macchia, A. Pizzabiocca, G. Renzi, M. Speranza, J. Chem. Soc. Chem. Commun. (1986) 458; (b) P. Crotti, F. Macchia, A. Pizzabiocca, G. Renzi, M. Speranza, Gazz. Chim. Ital. 117 (1987) 739; (c) P. Crotti, F. Macchia, A. Pizzabiocca, G. Renzi, M. Speranza, Tetrahedron Lett. 28 (1987) 3393; (d) P. Cecchi, A. Pizzabiocca, G. Renzi, M. Chini, P. Crotti, F. Macchia, M. Speranza, Tetrahedron 45 (1989) 4227; (e) P. Cecchi, M. Chini, P. Crotti, A. Pizzabiocca, G. Renzi, M. Speranza, Tetrahedron 47 (1991) 4683; (f) M. Chini, P. Crotti, F. Minutolo, E. Dezi, A. Lombardozzi, A. Pizzabiocca, G. Renzi, Tetrahedron 49 (1993) 5845.
[13] A. Troiani, A. Filippi, M. Speranza, Chem. Eur. J. 3 (1997) 2063.
[14] A. Filippi, M. Speranza, Int. J. Mass Spectrom. Ion Processes 185/186/187 (1999) 425.
[15] M. Aschi, M. Attinà, F. Cacace, Res. Chem. Intermed. 22 (1996) 645.
[16] M. Aschi, F. Cacace, A. Troiani, Angew. Chem. Int. Ed. Engl. 36 (1997) 83.
[17] (a) T.H. Morton, Tetrahedron 38 (1982) 3195; (b) D.J. McAdoo, T.H. Morton, Acc. Chem. Res. 26 (1993) 295.
[18] (a) M. Speranza, A. Filippi, Chem. Eur. J. 5 (1999) 834; (b) M. Speranza, A. Filippi, Chem. Eur. J. 5 (1999) 845.
[19] I.H. Chu, D.V. Dearden, J.S. Bradshaw, P. Huszthy, R.M. Izatt, J. Am. Chem. Soc. 115 (1993) 4318.
[20] R.B. Davidson, J.S. Bradshaw, B.A. Jones, N.K. Dalley, J.J. Christensen, R.M. Izatt, F.G. Morin, D.M. Grant, J. Org. Chem. 49 (1984) 353.
[21] D.V. Dearden, C. Dejsupa, Y. Liang, J.S. Bradshaw, R.M. Izatt, J. Am. Chem. Soc. 119 (1997) 353.
[22] J. Ramirez, F. He, C.B. Lebrilla, J. Am. Chem. Soc. 120 (1998) 7387.
[23] E. Camara, M.K. Green, S. Penn, C.B. Lebrilla, J. Am. Chem. Soc. 118 (1996) 8751.
[24] D.E. Clemmer, R.R. Hudgins, M.F. Jarrold, J. Am. Chem. Soc. 117 (1995) 10 141.
[25] W. Shen, P.S.H. Wong, R.G. Cooks, Rapid Commun. Mass Spectrom. 11 (1997) 71.
[26] R.G. Cooks, J.S. Patrick, T. Kotiaho, S.A. McLuckey, Mass Spectrom. Rev. 13 (1994) 287.
[27] W.A. Tao, D. Zhang, F. Wang, P.D. Thomas, R.G. Cooks, Anal. Chem. 71 (1999) 4427.
[28] (a) V.A. Davankov, J. Chromatogr. A 666 (1994) 55; (b) G. Gubitz, W. Jellenz, W. Santi, J. Chromatogr. A 203 (1981) 377.
[29] K. Vékey, G. Czira, Anal. Chem. 69 (1997) 1700.

[30] K. Vékey, G. Czira, Rapid Commun. Mass Spectrom. 9 (1995) 783.
[31] T. Vaisar, J. Urban, H. Nakanishi, J. Mass Spectrom. 31 (1996) 937.
[32] B. Brutschy, Chem. Rev. 92 (1992) 1567.
[33] H.J. Neusser, H. Krause, Chem. Rev. 94 (1994) 1829.
[34] (a) A.R. Al-Rabaa, E. Bréhéret, F. Lahmani, A. Zehnacker, Chem. Phys. Lett. 237 (1995) 480; (b) A.R. Al-Rabaa, K. Le Barbu, F. Lahmani, A. Zehnacker-Rentien, J. Phys. Chem. 101 (1997) 3273; (c) K. Le Barbu, V. Brenner, Ph. Millié, F. Lahmani, A. Zehnacker-Rentien, J. Phys. Chem. 102 (1998) 128.
[35] (a) S. Piccirillo, C. Bosman, D. Toja, A. Giardini Guidoni, M. Pierini, A. Troiani, M. Speranza, Angew. Chem. Int. Ed. Engl. 36 (1997) 1729; (b) A. Giardini Guidoni, S. Piccirillo, Isr. J. Chem. 37 (1997) 439; (c) A. Giardini Guidoni, S. Piccirillo, A. Palleschi, D. Toja, Proc. Indian Acad. Sci. (Chem. Sci.) 110 (1998) 1; (d) A. Latini, D. Toja, A. Giardini Guidoni, A. Palleschi, S. Piccirillo, M. Speranza, Chirality 11 (1999) 376.
[36] M. Satta, A. Latini, S. Piccirillo, T.M. Di Palma, D. Scuderi, M. Speranza, A. Giardini, Chem. Phys. Lett. 316 (2000) 94.
[37] (a) A. Latini, D. Toja, A. Giardini Guidoni, S. Piccirillo, M. Speranza, Angew. Chem. Int. Ed. Engl. 38 (1999) 815; (b) A. Latini, M. Satta, A. Giardini Guidoni, S. Piccirillo, M. Speranza, Chem. Eur. J. 6 (2000) 1042.
[38] S.G. Lias, J.E. Bartmess, J.F. Liebman, J.L. Holmes, R.D. Levin, W.G. Mallard, J. Phys. Chem. Ref. Data 17 (1988) suppl. 1.
[39] J. Long, B. Munson, J. Am. Chem. Soc. 99 (1977) 6822.
[40] S.W. Benson, Thermochemical Kinetics, Wiley, New York, 1968.